Highlights:

- Metformin, pioglitazone, and glibenclamide were loaded into scaffolds by ES and PG.
- The combination therapies (CT) accelerated diabetic wound healing on type-1 diabetic rats.
- CT showed better regeneration and lower TNF-α and NF-κB levels than single drug therapies.
- The formation of the hair follicles started in 14 days only in CT.
- CT has good cytocompatibility with L929 cells and ideal area for the proliferation.

Graphical Abstract

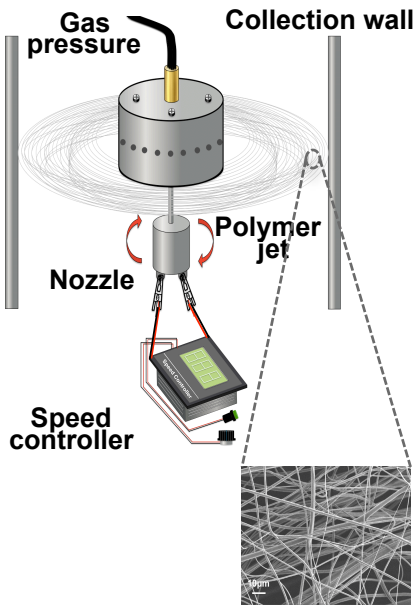

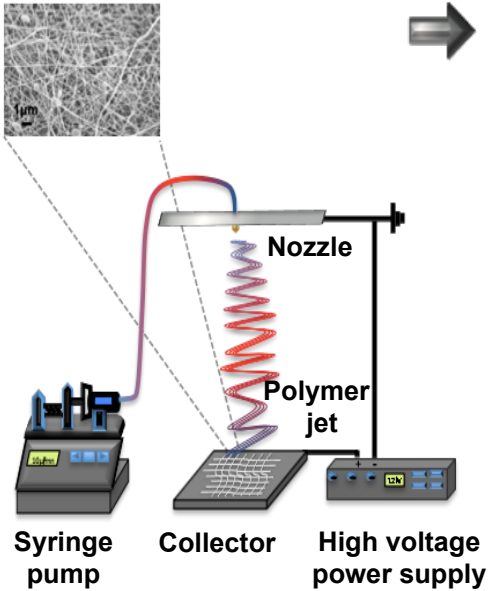

ELECTROSPINNING

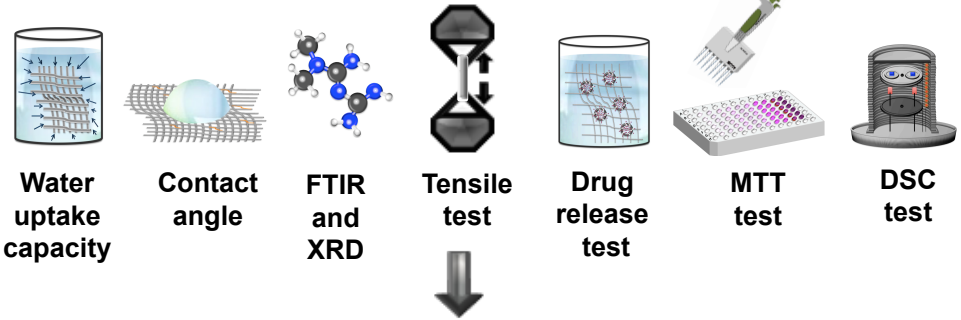

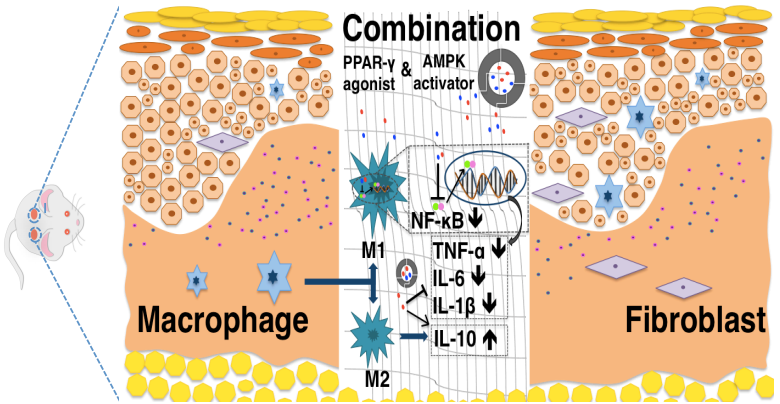

Manuscript File Click here to view linked References

Accelerated diabetic wound healing by topical application of combination oral antidiabetic agents-loaded nanofibrous scaffolds: An *in vitro* and *in vivo* evaluation study

Muhammet Emin Cam[a,b,c,*], Busra Ertas[c], Hussain Alenezi[a,d], Ayse Nur Hazar-Yavuz[c], Sumeyye Cesur[b,e], Gul Sinemcan Ozcan[f], Ceyda Ekentok[g], Ece Guler[b,c], Christina Katsakouli[a], Zehra Demirbas[h], Dilek Akakin[f], Mehmet Sayip Eroglu[i,j], Levent Kabasakal[c], Oguzhan Gunduz[b,e], Mohan Edirisinghe[a,*]

[a]Department of Mechanical Engineering, University College London, Torrington Place, London WC1E 7JE, UK

[b]Center for Nanotechnology and Biomaterials Application and Research, Marmara University, Istanbul 34722, Turkey

[c]Department of Pharmacology, Faculty of Pharmacy, Marmara University, Istanbul 34716, Turkey

[d]Department of Manufacturing Engineering, College of Technological Studies, PAAET, 13092 Kuwait City, Kuwait

[e]Department of Metallurgy and Material Engineering, Faculty of Technology, Marmara University, Istanbul 34722, Turkey

[f]Department of Histology and Embryology, Faculty of Medicine, Marmara University, Istanbul 34854, Turkey

[g]Department of Pharmaceutical Biotechnology, Faculty of Pharmacy, Marmara University, Istanbul 34722, Turkey

[h]Department of Clinical Microbiology and Infectious Diseases, School of Medicine, Gazi University, Ankara 06510, Turkey

[i]Department of Chemical Engineering, Faculty of Engineering, Marmara University, Istanbul 34722, Turkey

[j]Chemistry Group Laboratories, TUBITAK-UME, Kocaeli 41470, Turkey

*Corresponding authors. Tel.: +44 (0)20 7679 7062; fax: +44 (0)20 7388 0180

E-mail addresses: m.cam@ucl.ac.uk (M.E. Cam), m.edirisinghe@ucl.ac.uk (M. Edirisinghe)

ABSTRACT

The combination of oral antidiabetic drugs, pioglitazone, metformin, and glibenclamide, which also exhibit the strongest anti-inflammatory action among oral antidiabetic drugs, were loaded into chitosan/gelatin/polycaprolactone (PCL) by electrospinning and polyvinyl pyrrolidone (PVP)/PCL composite nanofibrous scaffolds by pressurized gyration to compare the diabetic wound healing effect. The combination therapies significantly accelerated diabetic wound healing in type-1 diabetic rats and organized densely packed collagen fibers in the dermis, it also showed better regeneration of the dermis and epidermis than single drug-loaded scaffolds with less inflammatory cell infiltration and edema. The formation of the hair follicles started in 14 days only in the combination therapy and lower proinflammatory cytokine levels were observed compared to single drug-loaded treatment groups. The combination therapy increased the wettability and hydrophilicity of scaffolds, demonstrated sustained drug release over 14 days, has high tensile strength and suitable cytocompatibility on L929 (mouse fibroblast) cell and created a suitable area for the proliferation of fibroblast cells. Consequently, the application of metformin and pioglitazone-loaded chitosan/gelatin/PCL nanofibrous scaffolds to a diabetic wound area offer high bioavailability, fewer systemic side effects, and reduced frequency of dosage and amount of drug.

KEYWORDS: Diabetic wound healing; Pioglitazone; Metformin; Glibenclamide; drug delivery; pressurized gyration; electrospinning

1. Introduction

Diabetes mellitus (DM) is a group of metabolic disorders, which is characterized by hyperglycemia following insulin resistance and/or deficiency in insulin secretion.[1] Long-term high blood glucose levels can cause dysfunction and failure of various organs.[2] As reported by World Health

Organization (WHO), 422 million people have diabetes worldwide and 200 million people are severely affected by both short-term and long-term complications.[3, 4]

One of the most common serious complications of diabetes is non-healing wounds, which also include diabetic ulcers, and these wounds may generate problems such as poor quality of life, severe infections, and amputation.[5, 6] The non-healing of diabetic wounds is the most frequent cause of hospitalization and the total cost of chronic wounds to the medical system is over US$25 billion per year.[7, 8] There are multiple factors such as abnormal inflammatory retention and reduced granulation tissue state which delay wound healing in DM and these factors are mainly arise from impaired glucose metabolism and also neurovascular complications.[9]

The inflammatory phase in diabetic wounds is characterized by hemostasis, chemotaxis, recruitment of neutrophils and macrophages, increasing vascular permeability, closing the wound, removing cellular debris and bacteria via phagocytosis, releasing reactive oxygen species (ROS) and matrix metalloproteinases, and fostering cellular migration. There is a sensitive balance in the number of free radicals, which has pro-mitogenic and antimicrobial features, on wound healing. The duration of the inflammatory stage usually lasts several days.[10]

The proliferative phase begins by migration of keratinocytes and is characterized by the generation of granulation tissue, reepithelialization, neovascularization, and eventually the ROS level decreases. The defects in phagocytosis and T-cell immunity provoke insufficient bacterial clearance, induce permanent altitude of proinflammatory mediators such as interleukin-6 (IL-6), tumor necrosis factor alpha (TNF-α), etc. Hyperglycemia-induced ROS firmly increase the number of inflammatory macrophage phenotypes associated with maintained inflammasome activity and creates a prolonged inflammatory stage. The proliferative phase can last for several weeks.[11-14] Tissue remodeling starts with the replacement of granulation tissue with scar tissue almost 3 to 6 weeks post-wounding and can last for months in the maturation phase.[15] On the other hand, endothelial dysfunction is strongly associated with the main reason of impaired wound healing ability.[16] As a result, the combinations of effective drugs, which have different mechanisms, can

be easily added to the novel therapeutic approaches with the development of technology to optimize the treatment of diabetic wounds.

Gelatin (GEL) is a protein derived from partial hydrolysis of collagen.[17, 18] Chitosan (CS) is especially attractive due to its broad antimicrobial spectrum and high biodegradability.[19, 20] Hence, electrospun GEL and CS complex can further mimic the composition of natural extracellular matrix (ECM). Polycaprolactone (PCL) and polyvinyl pyrrolidone (PVP) are FDA approved hydrophilic synthetic polymers, PCL-drug composite nanofibrous scaffolds have been used for wound healing materials due to its controlled release features.[21-23] In our study, GEL and CS composite were blended with PCL by electrospinning to achieve desired physical properties. Polyvinyl pyrrolidone (PVP)/PCL blends were also produced by pressurized gyration and they are also known for its aesthetic appearance, low chemical toxicity, physiological compatibility, and adhesion properties.[24]

In severe skin disorders such as diabetic foot ulcers, the treatment strategy is giving medications by oral route but also supportive topical treatments such as cream, ointment, and gel including antibiotics and anti-inflammatory agents [25]. Except for anti-inflammatory drugs, some hypoglycemic agents reduce inflammation that can contribute to improved outcomes. According to literature data, sulfonylureas, thiazolidinediones, dipeptidyl peptidase-4 inhibitors, and metformin (MET) with each of these classes of compounds exhibit moderate-to-strong anti-inflammatory effects.[26, 27] Therefore, MET, pioglitazone (PHR), and glibenclamide (GB), which also exhibit the strongest anti-inflammatory effect among antidiabetic drugs, were used in the current study to accelerate diabetic wound healing. Hence, fibrotic responses or tissue repair may be controlled in the future by the combination of thiazolidinediones, biguanides, and sulfonylureas that regulate PPAR-γ, AMPK, and K_{ATP} channel activity [28-30].

In the present study, we aimed to load different combinations of oral antidiabetic agents with PHR such as PHR&MET and PHR&GB into nanofibrous scaffolds. These drugs separately and in combination were loaded into two different polymer composites, CS/GEL/PCL and PVP/PCL, by

two different techniques, electrospinning and pressurized gyration. Thereafter, the biological impacts were examined in a wound healing test on type-1 diabetic rats for 14 days and also biochemical and histological analysis were done at the wound area. Additionally, morphological evaluation, physical and chemical composition, wettability and water uptake capacity (WUC), thermal properties, drug release behaviors of virgin CS/GEL/PCL nanofibrous scaffolds (V3S), MET-loaded CS/GEL/PCL nanofibrous scaffolds (M3S), PHR-loaded CS/GEL/PCL nanofibrous scaffolds (P3S), and PHR&MET-loaded CS/GEL/PCL nanofibrous scaffolds (PM3S), virgin PVP/PCL nanofibrous scaffolds (V2S), PHR-loaded PVP/PCL nanofibrous scaffolds (P2M), and PHR&GB-loaded PVP/PCL nanofibrous scaffolds (PG2S) were investigated. The cell morphology and proliferation were also investigated in order to evaluate applications in tissue engineering.

2. Materials and methods

2.1. Materials

Gelatin (GEL, from bovine skin, type B), chitosan medium molecular weight (CS, Mw = 190,000-310,000 g mol^{-1}), polycaprolactone (PCL, Mw~80,000), polyvinyl pyrrolidone (PVP, Mw~1,300,000 g mol^{-1}), pioglitazone hydrochloride (PHR, Mw~392.90 g mol^{-1}), metformin hydrochloride (MET, Mw~166.00 g mol^{-1}), glibenclamide (GB, Mw ~ 494.00 g mol^{-1}), streptozotocin (STZ, Mw~265.22 g mol^{-1}), phosphate buffer saline (PBS, pH=7.4), acetic acid (Mw~60.05 g mol^{-1}), chloroform, methanol, and glutaraldehyde solution (25 wt.% in H_2O, Mw ~100.12) were purchased from Sigma-Aldrich (Poole, UK). All purchased materials were of the analytical grade. For MTT assay, Cell Proliferation Kit I (MTT) kit was purchased from Roche.

2.2. Preparation and characterization of solutions

GEL and CS was dissolved at 20% and 2.5% w/v, respectively in a mixture of acetic acid and distilled water (9:1, v/v), and PCL was dissolved at 20% w/v in pure acetic acid. All solutions were prepared separately and mixed at 60^{o}C.[31-34] After that CS and GEL complex solutions were

obtained at three different ratios (5:5, 6:4, and 7:3, v/v) and these complex solutions were mixed with PCL solution at two different ratios (1:1 and 2:1, v/v), thereby six different CS/GEL/PCL concentration ratios (5:5:10, 5:5:5, 6:4:10, 6:4:5, 7:3:10, and 7:3:5, respectively, v/v/v) were tried to fabricate ideal V3S. According to the results obtained by scanning electron microscopy (SEM), MET at a concentration of 40 mg/ml,[35] PHR at a concentration of 12 mg/ml,[36] and the combination of these drugs in the same concentrations were added to optimized polymer solution (CS/GEL/PC=6:4:5, v/v) and mixed for almost four hours at room temperature (25^{o}C) to fabricate M3S, P3S, and PM3S. The drugs were not added in the duration of the preparation process of polymer solution due to the high temperature to avoid deterioration of the drugs. PVP/PCL blended solutions were prepared by dissolving at a constant polymer concentration (12% w/v) but in three different ratios (w_{PVP}/w_{PCL}=6/4, 7/3 and 8/2) in a mixture of chloroform and methanol (4:1, v/v) to produce V2S. GB at a concentration of 4 mg/ml and PHR at a concentration of 12 mg/ml were added to the same polymer solutions (w_{PVP}/w_{PCL}=6/4, 7/3 and 8/2) and a mixture of solvents to fabricate P2S and PG2S and they were mixed for almost 12 hours to ensure complete dissolution at room temperature (25^{o}C). Physical parameters such as density, viscosity, surface tension, and electrical conductivity for the solutions were measured by density bottle (10 mL specific density bottle, Boru Cam Inc., Turkey), viscometer (Brookfield DV-111, Harlow, UK), force tensiometer (Kruss K9, Hamburg, Germany), and electrical conductivity probe (Cond 3110 SET 1, WTW, Germany). All the measurements were repeated three times at ambient temperature (25^{o}C). These equipments were calibrated prior to measurements.

2.3. Preparation and characterization of nanofibrous scaffolds

At the beginning, V3S at six different concentrations (5:5:10, 5:5:5, 6:4:10, 6:4:5, 7:3:10, and 7:3:5, respectively, v/v/v) were fabricated. M3S, P3S, and PM3S were fabricated according to the optimized results obtained from SEM for virgin fibrous scaffolds (CS/GEL/PC=6:4:5, v/v). All these fibers were fabricated by electrospinning at ambient temperature (25^{o}C) and humidity (42%). PG technique could not be used because of the high acetic acid content in the solutions. For the

electrospinning procedure, working distances from 150 to 250 mm, flow rates from 0.1 to 0.5 mL/h and applied voltages from 20 to 30 kV were tried in the production process and optimized conditions were used in the fabrication of nanofibrous scaffolds. V2S scaffolds in three different ratios (w_{PVP}/w_{PCL}=6/4, 7/3 and 8/2; 12% w/v) were prepared by PG. V2S samples were also produced by electrospinning in order to compare the size and morphology of nanofibrous scaffolds fabricated by PG at ambient temperature (25^{o}C) and humidity (42%). P2S and PG2S scaffolds were also fabricated at three different ratios (w_{PVP}/w_{PCL}=6/4, 7/3 and 8/2; 12% w/v). All fibers were produced by PG using a method described previously.[37] In brief, 3 ml of solutions were placed into an aluminum vessel and spun at a rotational speed of 36000 rpm and a working pressure of 0.1 MPa to produce fibrous scaffolds. For the electrospinning procedure for the generation of V2S, working distances between 80 and 150 mm, flow rates between 0.2 and 1.0 ml/hr, and voltages between 6 and 15 kV were tried and optimized values were found. Hence, the fibers produced by pressurized gyration were compared with electrospinning. Their material compositions were investigated using spectroscopic and thermal techniques.

2.4. Crosslinking of nanofibrous scaffolds

A vacuum desiccator was used in order to dry all scaffolds and thus, remove any solvent residue from them. Crosslinking of CS/GEL/PCL fibrous scaffolds were carried out using GTA vapor. The samples were kept in a sealed glass container, which consists of two parts. The apparatus that divided the glass container has a perforated structure and while samples were placed on the upper part, 10 ml of 5 wt% GTA solution was placed in a small glass container at the bottom. The whole system was placed in an oven at 40°C for 5 h to create GTA vapor for crosslinking. Afterwards, a vacuum desiccator was used for 3 days in order to remove any residual GTA from the crosslinked CS/GEL/PCL scaffolds. During this process, the samples were on their own production paper (waxed paper) and their initial dimensions were preserved in this way. Besides, the nanofibrous scaffolds were fixed to avoid size reduction during crosslinking.[38]

2.5. Scanning electron microscopy (SEM)

The size and morphology of nanofibrous scaffolds were examined with scanning electron microscopy (Hitachi VP-SEM S-3400N). The surface of nanofibrous scaffolds was coated with gold for 60 seconds. The average diameter and size distribution of nanofibrous scaffolds were ascertained by analyzing 100 fibers in randomly recorded SEM micrographs using image software ImageJ (Brocken Symmetry Software).

2.6. Fourier transform infrared spectroscopy (FTIR)

FTIR measurements were performed using Jasco FT/IR 4700 spectrometer and spectrographs were studied using OPUS Viewer version 6.5 software to analyze the molecular contents of fibrous scaffolds and to confirm the presence of PHR, MET and GB in the fibrous scaffolds.

2.7. X-ray powder diffraction (XRD)

D/Max-BR diffractometer (RigaKu, Tokyo, Japan) with Cu Kα radiation was used to analyze structure and crystalline forms of the nanofibrous scaffold contents. Analyses were performed at 40 mV and 30 mA over 2θ range of 5–60° at a rate of 2°/min. OriginPro 7.0 software (OriginLab Corporation, MA, USA) was used to convert the obtained data to diffractrograms and these were evaluated.

2.8. Differential scanning calorimetry (DSC)

Perkin Elmer Jade DSC (PerkinElmer Inc., Mass., USA) and Pyris software were used to perform DSC analysis. The system was set at a heating rate of 10 °C min^{-1} between 0 and 200°C under a dynamic argon atmosphere (20 ml min^{-1}) to investigate the thermal properties of nanofibrous scaffolds. The system was calibrated prior to measurements.

2.9. Tensile test

An Instron 4411 tensile test machine was used to measure and evaluate the tensile strength of nanofibrous scaffolds, and then Bluehill 2 software (Elancourt, France) was used to study the results. After six samples with 10 x 50 mm size from each set of the sample groups were taken, the thicknesses of each sample were measured using a digital micrometer (Mitutoyo MTI Corp., USA) and then, the tensile strength of samples was calculated. All samples were carefully placed into the system at both ends. A tensile test was applied to each sample under conditions of 5 mm min^{-1} test speed and 1-cm distance between grips.

2.10. Contact Angle

A DSA-100 optical contact-angle meter (Kruss Company, Ltd, Germany) was used to measure the water contact angles of nanofibrous scaffolds at room temperature. Samples with 10 mm × 10 mm dimensions were cut and placed on the testing plate; subsequently distilled water was gently dropped onto the surface. A video monitor (Nikon, P600) was used to measure the contact angles, hence wettability of all samples was determined. All measurements were done in triplicate.

2.11. Water Uptake Capacity (WUC)

The water uptake capacity experiments were performed for all samples. Electrospun nanofibrous scaffolds of 50 mg were placed in distilled water at 37°C. The samples were taken from the water after 0.5, 1, 2, 3, 8, and 24 h. Firstly, the surface water of the samples was removed using filter paper and then they were weighed. The WUC (g/g) was calculated by measuring the weight of the nanofibrous scaffolds before (W_b) immersing in water for various times, and immediately after (W_a) their removal from the water, according to Equation (1)

$$WUC\ (g/g) = ((W_a - W_b)/W_b) \quad (1)$$

2.12. Drug encapsulation efficiency

Encapsulation efficiency is described as the weight ratio of the amount of incorporated drug loaded in the nanofibrous scaffolds to the initial amount of drug used to make the formulation. The standard assay procedure used to designate MET and PHR content in the fibrous scaffolds is as follows. Briefly, the nanofibrous scaffolds dissolved completely in their mixture solvents and UV detection was at 216 nm for PHR,[39] 234 nm for MET,[40] and 240 nm for GB.[41] M3S, P3S, PM3S, P2S, and PG2S were weighed (5 mg) and dissolved in 10 ml of their solvent mixtures in a volumetric flask. The flask was stirred gently over 1 h to provide a complete dissolution of PHR, MET, GB and combination of these drugs from nanofibrous scaffolds into the solvent mixtures. 3 ml of solution was taken and detected using an UV-visible spectrophotometer at 216, 234, and 240nm (Jenway 6305, Bibby Scientific, Staffordshire, UK). The % encapsulation efficiency was calculated using Equation (2). All measurements were done in triplicate.

Encapsulation efficiency = mass of actual drug loaded in fibrous scaffolds

/mass of drug used in fibrous scaffolds fabrication x 100% (2)

2.13. In vitro drug release assay

Analysis was performed to investigate the release kinetics of PHR, MET, GB and the combination of these drugs from embedded CH/GEL/PCL and PVP/PCL nanofibrous scaffolds. In order to evaluate the drug release kinetics, M3S, P3S, PM3S, P2S, and PG2S were cut into 5 mg samples which were separately immersed in 100 mL of PBS (pH 7.4 at 37^{o}C) for a period of 14 days. Thus, it can be found theoretically what amount of drug will be released from the nanofibrous scaffolds during the animal tests. For drug-loaded nanofibrous scaffolds, at the defined time intervals (at the 2nd, 4th, 6th, and 8th hours of the first day and then every day for 14 days) 3 mL of solution was taken from each sample container and fresh PBS of the same volume was added to continue the release test. UV spectroscopy (Jenway 7315, Bibby Scientific, Staffordshire, UK) was used for detecting of

PHR, MET, and GB releasing profiles at 216, 234, and 240 nm. At the beginning of drug release tests, a linear calibration curve of standard solutions was created. Drug releasing behaviors of M3S, P3S, PM3S, P2S, and PG2S were analyzed.

2.14. In vitro drug release kinetics

Five popular mathematical models were used to describe and simulate the kinetics of drug release from each nanofibrous scaffolds. Krosmeyer-Peppas, zero order, first order, Higuchi, and Hixon-Crowell models were used to simulate the drug release kinetics [42].

The equations for Korsmeyer–Peppas (3), zero order (4), first order (5), Higuchi (6), and Hixon-Crowell (7) are represented as below, respectively:

$$Q = Kt^n \quad (3)$$

$$Q = K_0 t \quad (4)$$

$$\ln(1-Q) = -K_1 t \quad (5)$$

$$Q = K_h t^{1/2} \quad (6)$$

$$Q^{1/3} = K_{hc} t \quad (7)$$

where Q is the fractional amount of drug release at time t; K, K_0, K_1, K_h, and K_{hc} are the kinetic constants for Krosmeyer-Peppas, zero order, first order, Higuchi, and Hixon-Crowell models, respectively. n is the diffusion exponent which is indicative of the drug release mechanism.

2.15. Methylthiazolydiphenyl-tetrazolium bromide (MTT) viability assay

L929 cells were cultured in DMEM supplemented with 10% FBS then seeded in 48-well plates at a density of 2.5×10^4 cells/well and cultured overnight at 37°C and 5% CO_2. Cells were treated with each sample for 48 h. After 48 hours incubation, culture medium was replaced with fresh medium and 20 µl MTT solution was added in each well and the plate incubated at 37°C and 5% CO_2 for 4

h. After 4 hours, formazan crystals were solubilized by adding 200 µl solubilization buffer and spectrophotometrical absorbance measured at 550 and 690 nm. The confluent cells were used in cytotoxicity tests and also SEM investigations.

2.16. In vivo wound healing experiments

The permission for the animal experiments was granted by the Animal Experiments Local Ethics Committee at Marmara University (approval number: 113.2018.mar). Adult male and female Sprague-Dawley rats (300-350 g) (n=12 in each experiment) were purchased from Marmara University Experimental Animal Implementation and Research Center. The rats were housed under in regulated rooms with controlled temperature (20-23°C), humidity (40-60%) and light (12 h light/dark regime). A standard rodent pellet diet with tap water was available ad libitum to the animals.

2.16.1. Experimental design of wound healing experiment

Type-1 DM was induced in rats by a single intraperitoneal injection in 60 mg/kg body weight of streptozotocin (STZ), which was prepared in sodium citrate buffer (0.1 mol/L, pH 4.5) immediately before using, following overnight fasting. The diabetic status was confirmed 72 h after STZ injections by measuring the blood glucose level collected from tail vein with blood glucose strips (Contour^{TM} PLUS, Bayer Diagnostics). Rats with blood glucose levels greater than 300 mg/dl were considered diabetic and included in the experiment. 10 days after the STZ administration, wound formation studies were performed. In order to begin the experiments, rats were kept for 10 days to obtain a chronic hyperglycemic state [43-45].

After anesthetic administration with intraperitoneal injection of 10 mg/kg xylazine hydrochloride (Rompun) and 25 mg/kg ketamine hydrochloride (Ketalar), the dorsal hair of diabetic rats was completely shaved and the skin was disinfected with povidone-iodine. A sterile biopsy skin punch with a diameter of 8.0 mm (Kai Medical, BP-80F Japan) was utilized on both sides of the middle

back of each rat and a full-thickness wound to the deep fascia was created according to the template.[46] The rats were divided into 8 groups, each of 12 rats: 1. Control group (no treatment), 2. V3S group (treated with fiber carrying no active drug), 3. M3S group (treated with only MET-loaded fiber drug), 4. P3S group (treated with only PHR-loaded fiber), 5. PM3S group (treated with combination of PHR&MET-loaded fiber), 6. V2S group (treated with virgin PVP/PCL fiber); 7. P2S group (treated with PHR-loaded PVP/PCL fiber); 8. PG2S group (treated with PHR&GB-loaded PVP/PCL fibrous scaffolds). During the healing process, no dressings were changed and no other topical medication was applied. Rats were kept in pairs after surgical incisions. Wound margins were observed and photographed on different days (0^{th}, 3^{rd}, 7^{th}, 10^{th}, 12^{th}, and 14^{th} day after surgical incision) in order to monitor the changes in the size of the wounds. The original area (day 0 area) was identified as the area identified by the trace obtained immediately after wounding. Wound closure is expressed as percentage closure relative to original size and was calculated according to Equation (3).

$$\% \text{ Wound closure} = 100 \times (\text{Initial wound area} - N^{th} \text{ day wound area})/(\text{Initial wound area}) \quad (3)$$

N varies between 0 and 14.

In all groups, the body weight of rats was strictly monitored. The blood of rats was obtained from a tail vein and its glucose level was measured using blood glucose strips. Insulin glargine therapy was given in the case of rats losing weight and/or had high glucose levels (Sanofi-Aventis, Frankfurt, Germany).

At days 3, 7, and 14, the animals were sacrificed and the entire wound area was collected for further studies. For histopathology, the tissues were embedded in %10 formalin solutions. Additionally, on 14^{th} day, the removed wounded area was stored at -80°C for biochemical studies.

2.16.2. Implantation of fibrous scaffolds into the rats

In order to determine the therapeutic effects of each sample on diabetic wound healing, the wounds

were completely covered with nanofibrous scaffolds (diameter of 8 mm). After covering, the wounds were wrapped with 3M Tegaderm elastic bands (22 mm x 22 mm, Tegaderm^{TM}, 3M Health Care, Germany) for a day. A self-adhering cover (Nexcare^{TM}, 3M Health Care) was used for several hours to ensure that the nanofibrous scaffolds remained on the wounds.

2.17. Biochemical analysis

Wounded tissue samples were collected after decapitation. Rat wounds were homogenized and supernatant of the homogenates was analyzed using ELISA kits purchased by Bioassay Technology Laboratory, Korain Biotech Co., Ltd. (Shanghai, China). All procedures were carried out according to the instructions of the manufacturer.

2.18. Histopathological analysis

For histopathological observations, skin wound samples collected on days 3, 7, and 14 were immediately fixed in 10% neutral buffered formalin. Wound tissue samples were embedded in paraffin blocks and cut into 4 µm tissue sections. The sections were deparaffinized in xylene, hydrated, and stained with hematoxylin and eosin (H&E) to evaluate general morphology and with Gomori's trichrome stain to evaluate collagen fibers. Finally, sections mounted with a cover slip were observed under a light microscope (Olympus BX51, Tokyo, Japan). With respect to epidermal and dermal regeneration (1:little epidermal and dermal organization; 2:moderate epidermal and dermal organization; 3:complete remodeling of epidermis and dermis), inflammatory cell infiltration, granulation tissue formation and edema (0:none; 1:mild; 2:moderate; 3:severe) semiquantitative scoring was done and comparison was made between experimental groups by a histologist who was unaware of the experimental procedure. The wound length was measured on the pictures captured by camera using image J programme.

2.19. Statistical analysis

Scanning electron microscopy results are presented as mean ± standard deviation (SD). The

interactions between different groups in MTT test, animal test, histopathological and biochemical analysis were tested using analysis of variance (ANOVA) with 95% confidence interval and Bonferroni's post hoc test. The results were expressed as mean ± standard error mean, and values of $p > 0.05$ were not considered significantly different, whereas values of $p < 0.05$ were considered significant. Data analysis was performed using Graph Pad Prism 6.5 software (Graph Pad, San Diego, CA, USA).

3. Results and Discussion

3.1. Physical properties of solutions

Six different solutions of V3S and three different solutions of M3S, P3S, and PM3S were used. Various solutions were prepared to produce V2S, P2S, PG2S using pressurized gyration and electrospinning. The main parameters that affect the formation and homogeneity of nanofibrous scaffolds are ambient conditions such as temperature and humidity, process conditions such as working pressure and rotational speed for PG; working distance, polymer solution feed rate, applied voltage for electrospinning, solution properties such as viscosity, density, surface tension, and in addition for electrospinning, electrical conductivity.[47, 48] These parameters were recorded for each solution (Table S1a).

3.2. Process conditions

Two different production techniques were used in this study, electrospinning and pressurized gyration. The process parameters used in order to obtain ideal fiber morphologies and size for each set of samples were recorded (Table S1b, Supporting Information).

3.3. Morphological characterization of nanofibrous scaffolds

The changes in the morphology and fiber size of virgin CS/GEL/PCL fibrous scaffolds at six different ratios and M3S, P3S, and PM3S were analyzed using SEM. Primarily, the optimized CS/GEL/PCL concentration was determined to use the same ratio for drug loading, virgin fibrous

scaffolds at six different concentrations (5:5:10, 5:5:5, 6:4:10, 6:4:5, 7:3:10, and 7:3:5, v/v/v) were fabricated using electrospinning (Figure 1).

The decrease of GEL in the composite fibers caused the morphology to deteriorate. Besides, at the higher ratio of CS defects were present in the composite fibers, while these defects almost disappeared at equal ratio of CS and GEL. However, the diameter of the composite fibers decreased with the decrease of GEL ratio. The minimum amount of GEL was in the 7:3:10 (CS/GEL/PCL) ratio and the diameter of the fibers was φ=125.2 ± 38.3 nm, which was the smallest diameter obtained from virgin nanofibrous scaffolds. The maximum amount of GEL was in the 5:5:5 (CS/GEL/PCL) ratio and the diameter of the fibers was φ=227.5 ± 134.5 nm, which was the greatest diameter obtained from virgin nanofibrous scaffolds. At two different ratios, which are 5:5:10 (φ=158.3 ± 67.8 nm) and 6:4:5 (φ=138.0 ± 42.5 nm), we achieved ideal morphology, beadless and uniform fibers, but the 6:4:5 ratio was chosen for the further studies due to the higher ratio of CS and GEL, and also smaller diameter.

It is known that with the increase in electrical conductivity and decrease in surface tension, smaller diameter of fiber can be obtained.[49] After the determination the polymer ratio according to virgin fibrous scaffolds, drugs were loaded into the same ratio of polymers (CS/GEL/PCL = 6:4:5, v/v/v). Depending on high electrical conductivity and low surface tension, the diameter of M3S (φ=56.4 ± 22.9 nm), P3S (φ=46.4 ± 14.7 nm), and PM3S (φ=64.3 ± 17.1 nm) were smaller compared to virgin nanofibrous scaffolds (Figure 1g-i). Fiber diameter distributions are given in Figure S2. When we analyze the morphology of fibers, it can be seen that MET, PHR and the combination of these drugs were encapsulated successfully inside fibers, and more evidence for this is discussed below. Besides, Figure 1j-l demonstrates the morphology of nanofibrous scaffolds after GTA vapor crosslinking. The co-existence of moisture with GTA vapor during the crosslinking process altered the fiber morphologies to some extent. The water-resistance capacity was improved by crosslinking.

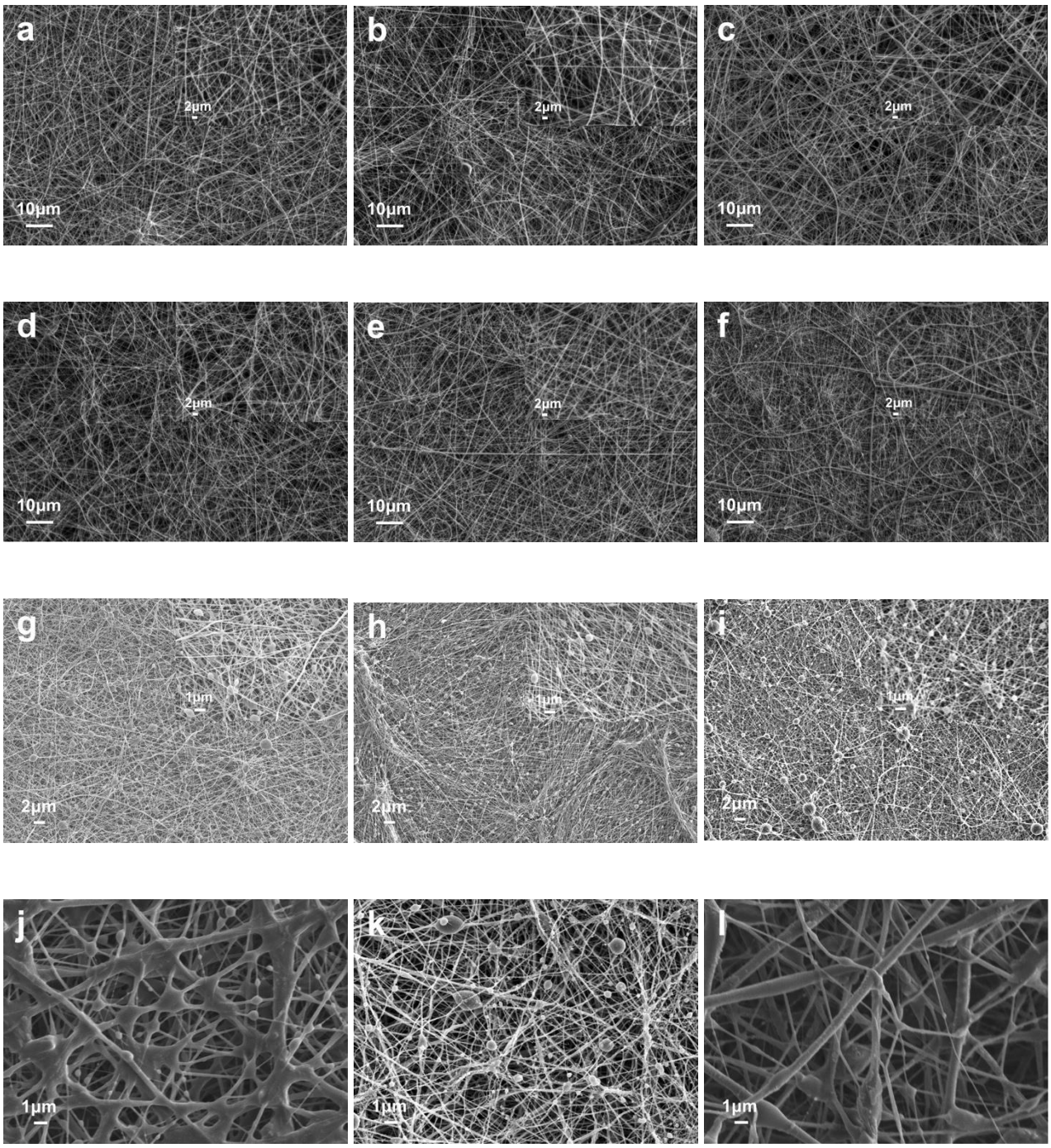

Figure 1. SEM images and fiber diameter distribution of virgin CS/GEL/PCL fibrous scaffolds at six different ratios: (a) 5:5:10, (b) 5:5:5, (c) 6:4:10, (d) 6:4:5, (e) 7:3:10, and (f) 7:3:5 (v/v/v) and (g) MET-loaded CS/GEL/PCL, (h) PHR-loaded CS/GEL/PCL, (i) MET&PHR-loaded CS/GEL/PCL, and after glutaraldehyde vapor crosslinking: (j) MET-loaded CS/GEL/PCL, (k) PHR-loaded CS/GEL/PCL, and (l) MET&PHR-loaded CS/GEL/PCL. All were fabricated by electrospinning.

The changes in fiber size and morphology of V2S, P2S and PG2S fabricated by pressurized gyration and electrospinning were investigated using SEM. First, virgin fibers with three different

ratios (w_{PVP}/w_{PCL}=6/4, 7/3 and 8/2; 12% w/v) were produced and compared with electrospinning to see whether we could obtain fibers with similar morphology, diameter and distribution with pressurized gyration. According to the results obtained from pressurized gyration and electrospinning for the production of V2S, the fiber diameter for 6/4 (w_{PVP}/w_{PCL}) polymer ratio is 821.5 ± 521.9 nm by pressurized gyration and 608.1 ± 277.2 nm by electrospinning, for 7/3 (w_{PVP}/w_{PCL}) polymer ratio 820.6 ± 376.9 nm by pressurized gyration and 683.3 ± 261.2 nm by electrospinning, for 8/2 (w_{PVP}/w_{PCL}) polymer ratio 740.4 ± 330.4 nm by pressurized gyration and 746.0 ± 210.5 nm by electrospinning. The fiber diameter distribution is more monodisperse for electrospinning compared to pressurized gyration at all concentrations but fiber size was similar in the 8/2 (w_{PVP}/w_{PCL}) polymer ratio, therefore V2S in this ratio were chosen for further studies. Bead and droplet defects were not observed in all samples (Figure 2a-f).

It is well known that fiber dissolution rate and drug release characteristics can be adjusted by controlling some variables such as fiber diameter. Briefly, a greater fiber diameter accompanies lower surface area and would cause the drug release to be delayed compared to the smaller diameter. In order to make a clear comparison between the polymer ratios, it was decided to produce fibers with ratio 6/4 (w_{PVP}/w_{PCL}) for PHR and 8/2 (w_{PVP}/w_{PCL}) for the combination of PHR&GB by pressurized gyration. The diameter of fibers decreased slighlty by adding PHR (813.5 ± 256.9 nm) compared to its virgin form (Figure 2g). On the other hand, the diameter of fibers increased by adding the combination of GB&PHR (779.1 ± 276.9 nm) compared to its virgin form (Figure 2h).

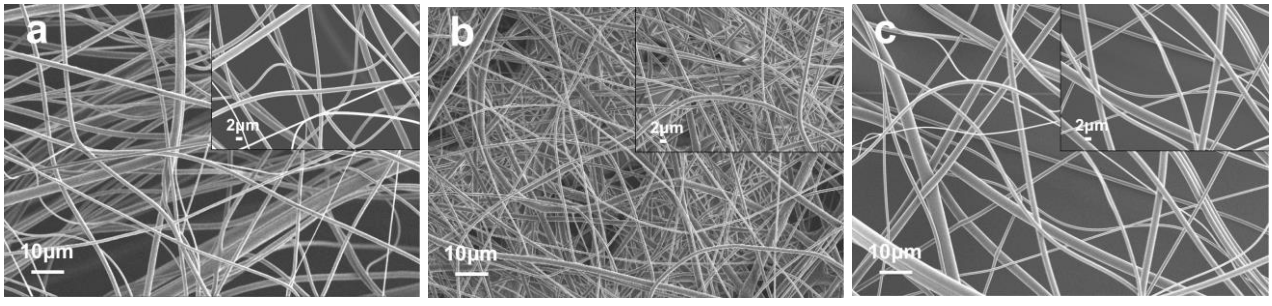

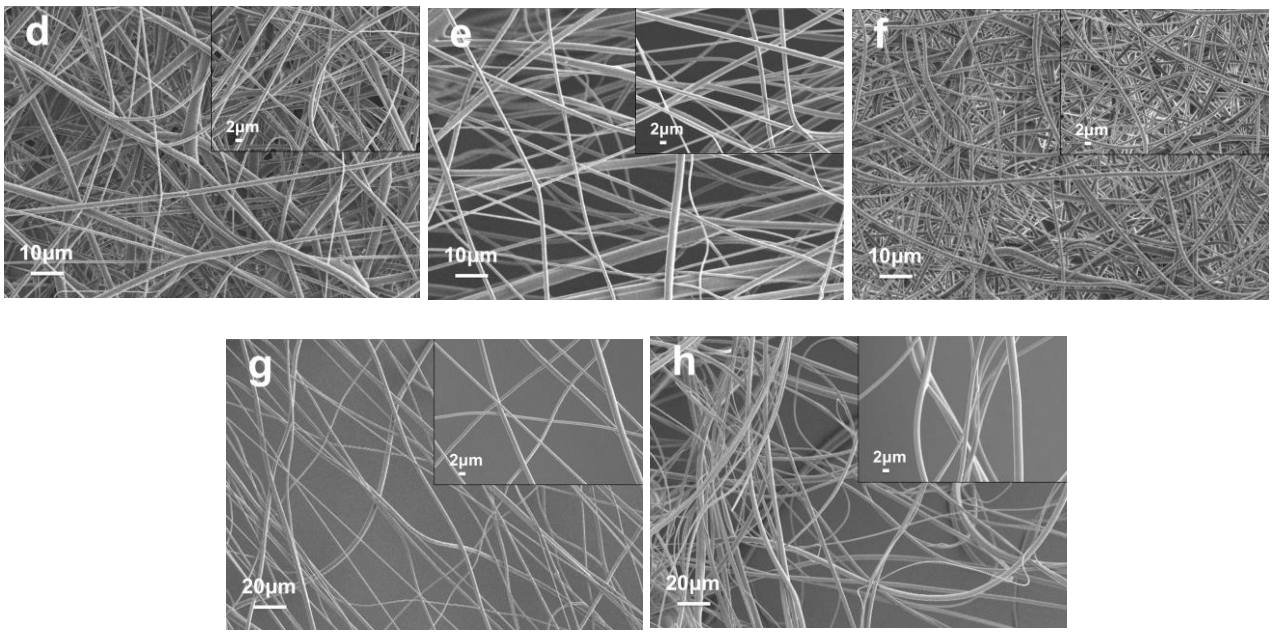

Figure 2. SEM images of virgin PVP/PCL (12%, w/v) nanofibrous scaffolds: w_{PVP}/w_{PCL}=6/4 PVP/PCL by pressurized gyration (a) and by electrospinning (b), w_{PVP}/w_{PCL}=7/3 PVP/PCL by pressurized gyration (c) and by electrospinning (d), w_{PVP}/w_{PCL}=8/2 PVP/PCL by pressurized gyration (e) and by electrospinning (f); PHR-loaded (w_{PVP}/w_{PCL}=6/4) PVP/PCL nanofibrous scaffolds by pressurized gyration (g) and PHR&GB-loaded (w_{PVP}/w_{PCL}=8/2) PVP/PCL nanofibrous scaffolds by pressurized gyration.

3.4. Fiber composition

In order to analyze molecular contents of nanofibrous scaffolds, FTIR was used and it was proved that PHR, MET, and GB were encapsulated successfully into M3S, P3S, PM3S, P2S, and PG2S samples. The molecular structures of pure chitosan, gelatin, PVP, PCL, PHR, MET, and GB and also all nanofibrous scaffold samples prepared by electrospinning and pressurized gyration are given in Figure 3.

Many similar peaks were detected in FTIR results due to the common functional groups of chitosan and gelatin. For instance, a broad OH band at ~3300 cm^{-1} and a weak CH_2 peak at ~2900 cm^{-1} were exhibited in all samples.

C=O groups of acetylated amide and amine groups at 1650 and 1589 cm^{-1}, respectively, characteristic absorption bands at 1149 and 894 cm^{-1} due to saccharide groups, and characteristic C-O-C bonds at 1023 cm^{-1} were observed for pure CS.[50]

The C=O stretching band of amide I at 1627 cm^{-1}, N–H bending band of amide II at 1525 cm^{-1}, and N–H bending band of amide III at 1234 cm^{-1} belong to pure GEL.[51]

CH_2 asymmetric stretching bands at 2945 cm^{-1}, CH_2 symmetric stretching bands at 2866 cm^{-1}, characteristic C=O stretching peak at 1720 cm^{-1}, C-H group bending at 1471 and 1417 cm^{-1}, O-H bending at 1396 and 1364 cm^{-1}, C–O stretching band at 1293 cm^{-1}, C-O-C asymmetric stretching band at 1238 cm^{-1}, and C-O-C asymmetric and symmetric stretching band at 1165 cm^{-1} are assigned to PCL.[24, 52]

Peaks for pure PVP were measured at 3439 cm^{-1}, 2944 cm^{-1}, 1655 cm^{-1}, and 1492 cm^{-1} belongs to the O-H stretching vibrations band due to amide-iminol tautomerism, C-H asymmetric stretching band, the characteristic and also the most intensive absorption band amide C=O stretching vibration, and CH_2 scissoring, respectively. The peaks at 1459 and 1419 cm^{-1}; 1371 and 1314 cm^{-1}; 1282 and 1268 cm^{-1}; 1226 and 1166 cm^{-1} characterize C–N stretching vibrations, C-H bending bands, characteristic absorption bands of C–N stretching, and CH_2 twist bands, respectively.[24, 52]

The peaks of aliphatic C-H asymmetric and symmetric stretching at 2925 and 2740 cm^{-1}, respectively characterize pure PHR.[53] Characteristic peaks measured at 1741 cm^{-1}, 1509 cm^{-1}, 1242 cm^{-1} are assigned to amide C=O stretching, C=N stretching, and C-O stretching bands, respectively. Moreover, C=C stretching, ring C-N stretching, aliphatic C-O-C, and C-S stretching bands were detected at 1607 cm^{-1}, 1461 cm^{-1}, 1109 cm^{-1}, and 659 cm^{-1}, respectively.[54]

FTIR spectra for MET in fiber include; N-H stretching of primary amine group at 3145 cm^{-1}, C-N stretching/N-H bending/C=O stretching band at 1621 cm^{-1}, and N-H bending vibrations of the primary amine group at 1545 cm^{-1}.[55] Moreover two typical bands at 3366 and 3290 cm^{-1} due to N-H primary stretching vibration, CH_3 asymmetric bending vibration at 1472 cm^{-1}, C-H bending at 1445 cm^{-1}, CH_3 symmetric bending vibration at 1417 cm^{-1}, C-O stretching at 1166 cm^{-1} were

observed for MET.[56]

GB shows two characteristic peaks at 3365 and 3309 cm^{-1} that correspond to the amide stretching bands, CH=CH band at 2929 cm^{-1}, C=O stretching vibration at 1713 cm^{-1}, C=O stretching at 1615 cm-1, C=C stretching bands at 1591 and 1519 cm^{-1}, symmetric and asymmetric $S=O_2$ stretching at 1340 and 1155 cm^{-1}, respectively. [57, 58]

When compared, the spectrum of drug-loaded fibrous scaffolds samples to V3S, new peaks at 3145, 1621 and 1545 cm^{-1} are assigned to MET for M3S and PM3S samples and new peaks at 1741, 1509, and 1242 cm^{-1} belong to PHR for P3S and PM3S samples. For the V3S sample, peaks at 1149, 1023, and 894 cm^{-1} characterize CS and peaks at 1627, 1525 and 1234 cm^{-1} characterize GEL and peaks at 2945, 2866, and 1720 cm^{-1} characterize PCL (Figure 3a). In the PG2S absorbance spectrum, new peaks were observed at 3365 and 3309 cm^{-1} and are assigned to GB and 1741, 1509, and 1242 cm^{-1} belongs to PHR, compared with the V2S absorbance spectrum. For V2S composite sample, peaks at 2945, 2866, and 1720 cm^{-1} are assigned to PCL and the peaks at 1655 and 1282 cm^{-1} is assigned to PVP (Figure 3b). Thus, according to these results successful formulation and drug encapsulation was ensured.

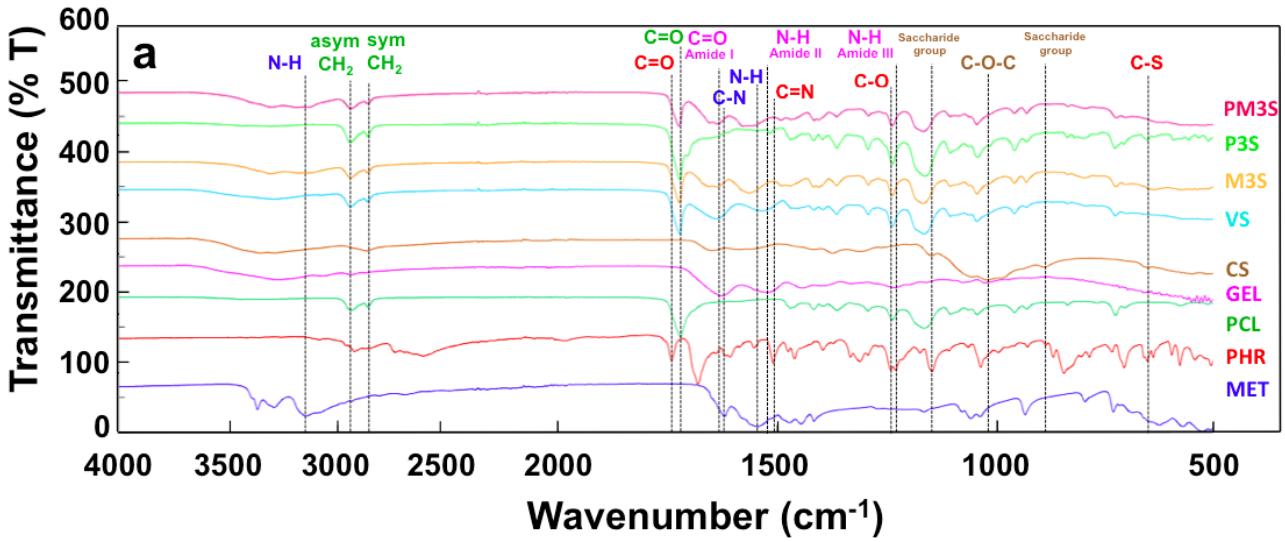

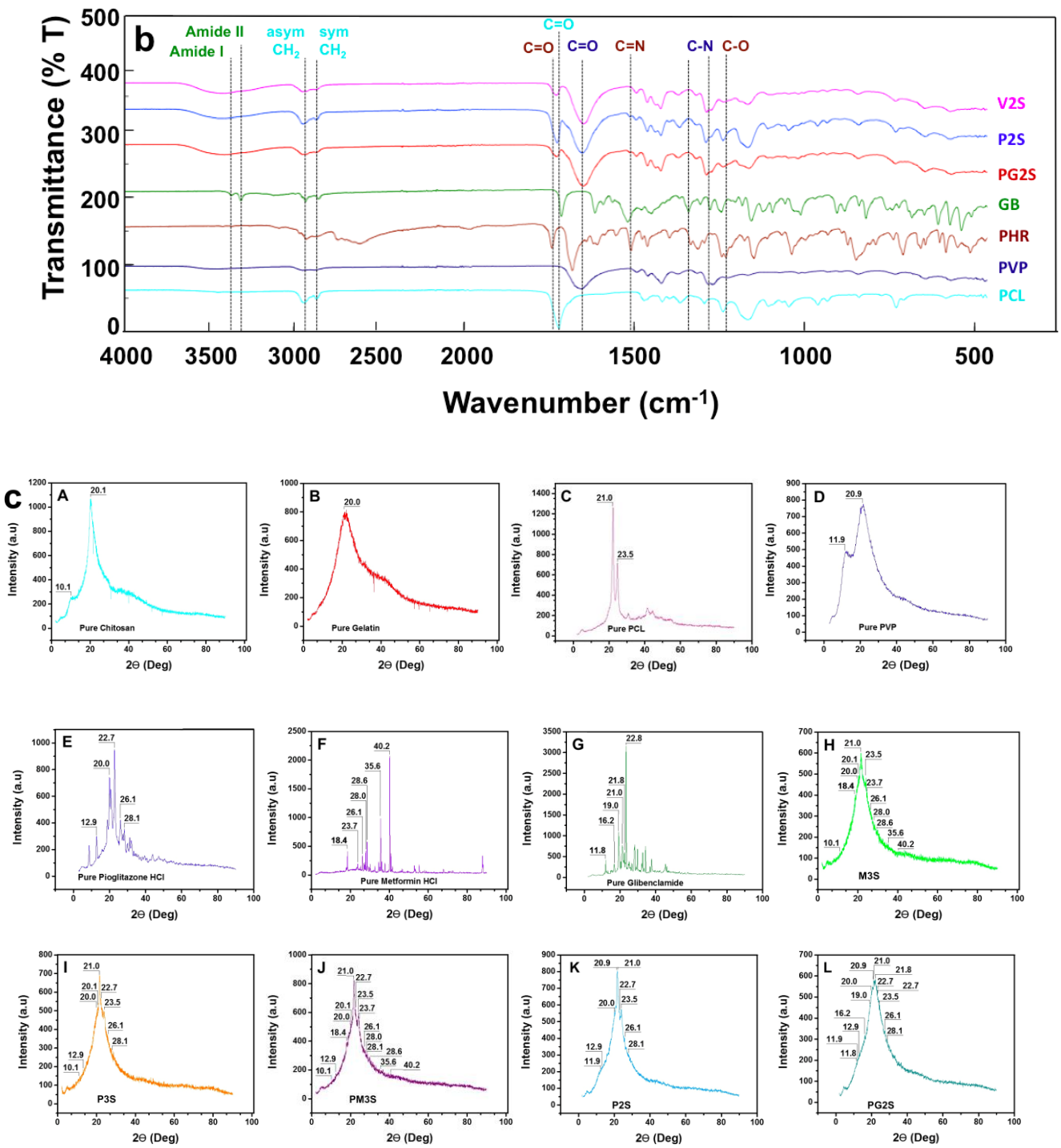

Figure 3. FTIR spectrums of (a) pure chitosan, gelatin, PCL, metformin HCl, pioglitazone HCl, and also nanofibrous scaffold samples: M3S, P3S, and PM3S; (b) pure PCL, PVP, PHR, GB, and GPNM, PNM, VNM. (c) XRD patterns of pure chitosan (A), pure gelatin (B), pure PCL (C), PURE PVP (D), pure pioglitazone HCl (E), pure metformin HCl (F), pure glibenclamide (G), M3S (H), P3S (I), PM3S (J), P2S (K), PG2S (L).

3.5. XRD analysis of nanofibrous scaffolds

XRD is a useful technique for analyzing the crystallinity in polymers. Figure 3c shows X-ray diffraction patterns of pure chitosan, gelatin, PVP, PCL, PHR, MET, GB, CS/GEL/PCL, and PVP/PCL nanofibrous scaffolds. Two diffraction peaks at 10.1° and 20.1° 2θ suggest the semi-crystalline nature of chitosan. A broader peak at 20.0° 2θ indicates the amorphous nature of gelatin. Two peaks at 21.0° and 23.5° 2θ show the crystalline nature of PCL.[59] Diffraction peaks at 11.9 and 20.9 2θ were observed for PVP.[60] Major peaks of MET were observed at 18.4, 23.7, 26.1, 28.0, 28.6, 35.6, and 40.2 2θ;[61] PHR showed major peaks at 12.9, 20.0, 22.7, 26.1, and 28.1 2θ;[62] and GB at 11.8, 16.2, 19.0, 21.0, 21.8, and 22.8 2θ.[63] According to XRD results, practically existing compounds were detected in all samples. A decrease in the degree of crystallinity of the nanofibrous scaffolds was observed due to the reduced intensity of PCL peaks with the incorporation of amorphous GEL and semi-crystalline CS in PCL. This situation indicates some interactions prevailed among the molecules of CS, GEL, and PCL.[59] However, these interactions were not detrimental to the results of this study.

3.6. Tensile properties of nanofibrous scaffolds

The mechanical properties of all samples were measured using a tensile tester. Figure 4a shows the tensile strength and strain at break of all samples. The experimental results show that CS/GEL/PCL samples have greater tensile strength than PVP/PCL samples and P3S is the most durable compared to others. Loading drug in CS/GEL/PCL nanofibrous scaffolds increased the tensile strength but in the case of the combination of drugs the increase was lower than both single drug-loaded scaffolds. V2S in both ratios have greater tensile strength than P2S and PG2S. V2S in 6/4 (w_{PVP}/w_{PCL}) ratio is stronger than 8/2 (w_{PVP}/w_{PCL}) ratio, hence it can be said that the increase of PCL ratio in the composite makes it stronger. Similar results and trends were seen from the strain at break.

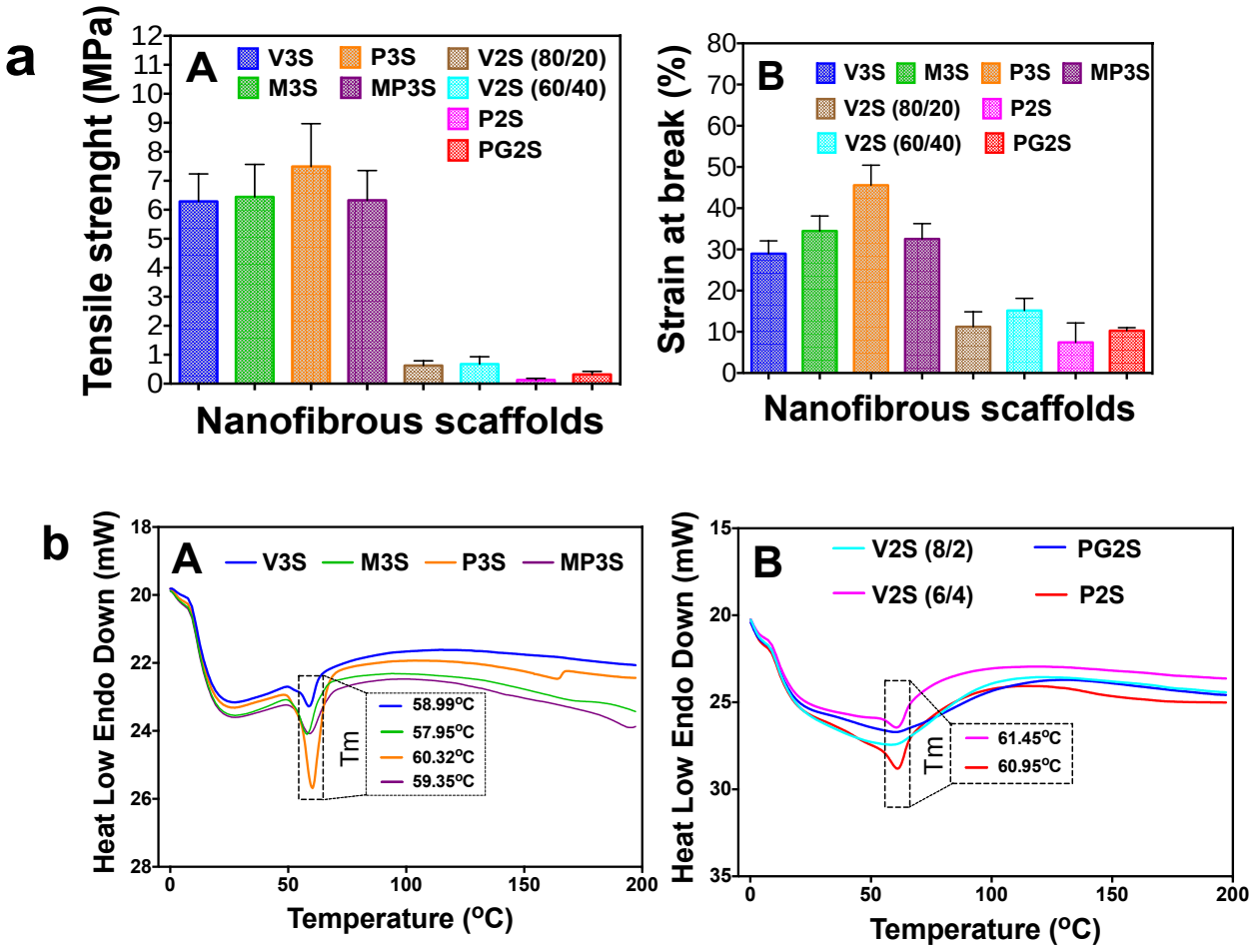

Figure 4. Mechanical (a) and physical (b) parameters of nanofibrous scaffolds: (A) tensile strength and (B) strain at break. DSC curves of (A) V3S, M3S, P3S, PM3S and (B) V2S (8/2), V2S (6/4), P2S, PG2S.

3.7. Melting behaviour of nanofibrous scaffolds

DSC is a useful technique to determine any physical changes of materials accompanied by heat absorption or release. In this study, the effect of drugs on the melting point of nanofibrous scaffolds consisting of CS/GEL/PCL and PVP/PCL, and thus their intermolecular interactions were investigated. The DSC curves of virgin and drug-loaded nanofibrous scaffolds recorded in the temperature range 0-200°C are presented in Figure 4b. CS and GEL did not exhibit melting behavior in this temperature range and thus, the endothermic peak observed at 59.0°C in the DSC curve of virgin PCL/CS/GEL was attributed to PCL melting in the nanofibrous composite. Melting point of PCL was determined as 58.0°C for M3S, 59.4°C for MP3S, and 60.3°C for P3S. It is

notable that, melting point of PCL in P3S increased very slightly while for M3S it decreased slightly. Additionally, the PCL melting point was between those temperatures in the presence of MP3S (Figure 4b-A). This could be explained by the strong hydrogen bonding formed between amine groups of PHR and carbonyl groups of PCL. As shown in Figure 4b-B, the Tm of the V2S (6/4) composites were approximately 60°C, which is the almost the same Tm for pure PCL. While the Tm value of V2S (6/4) was 61.45°C, that of P2S was 60.95°C. Tm value of composite scaffold was slightly decreased by the addition of PHR. The Tm value could not be detected in V2S (8/2) and PG2S samples have a very amorphous structure due to high PVP ratio (Figure 4b-B). These results indicate that all nanofibrous scaffold samples can be safely applied in wound sites without risk of melting.

3.8. Water uptake capacity of nanofibrous scaffolds

Nanofibrous scaffolds with favorable water-holding capacity absorb the wound exudate and helps to keep the environment moist in order to promote nutrient transport and cell signal transfer. Thus, cell growth and proliferation are improved and as a result, wound healing is accelerated. Hence, water-holding capacity was investigated as an important indicator of scaffolds.[64] Nanofibrous scaffolds grow rapidly with the increase of immersing time in 24 hours. The water absorption content of all samples increased with time and reached their peak values of 10.34 ± 0.93, 8.65 ± 0.78, 10.52 ± 0.95, 8.43 ± 0.76, 2.39 ± 0.22, and 2.95 ± 0.27 g g^{-1} for V3S, M3S, P3S, PM3S, V2S (6/4), P2S, respectively, at 24 hours (Figure 5a). The water absorption values of V2S (8/2) and PG2S samples were quite low due to their high PVP ratio in the PVP/PCL composite fiber. Thus, the 8/2 ratio for PVP/PCL composite polymer is not effective for holding water. P2S samples kept almost three times water as its initial weight in 24 hours. It is also confirmed that all CS/GEL/PCL nanofibrous scaffolds have favorable water holding capacity and can absorb a minimum 8-fold compared to their starting weight in 24 hours. It was clearly seen that the addition of GB and PHR increased water absorption, conversely MET decreased it. The combination of the two drugs decreased the water absorption capacity less only in the case of MET.

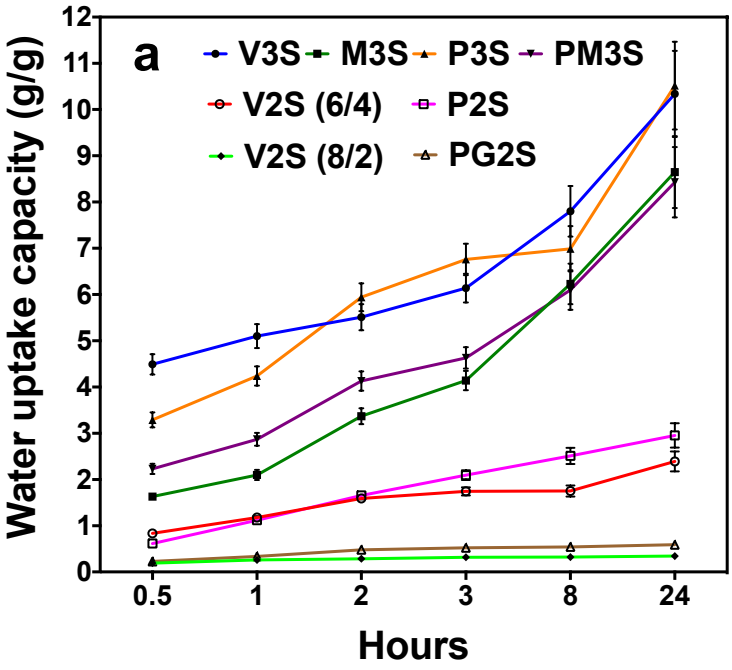

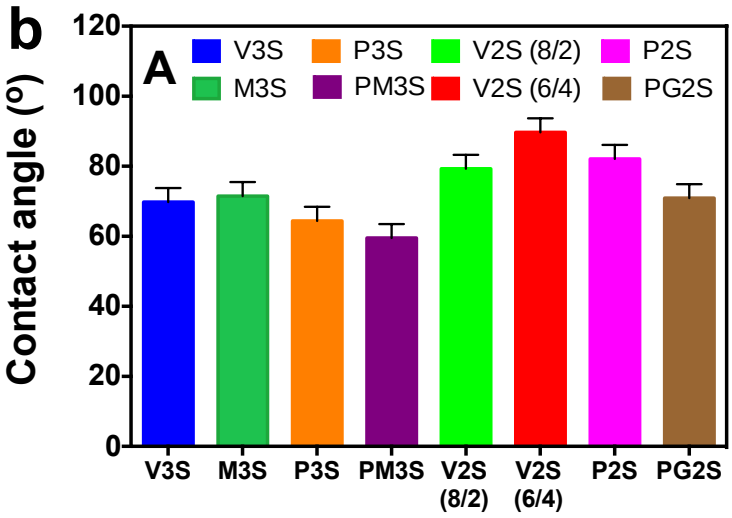

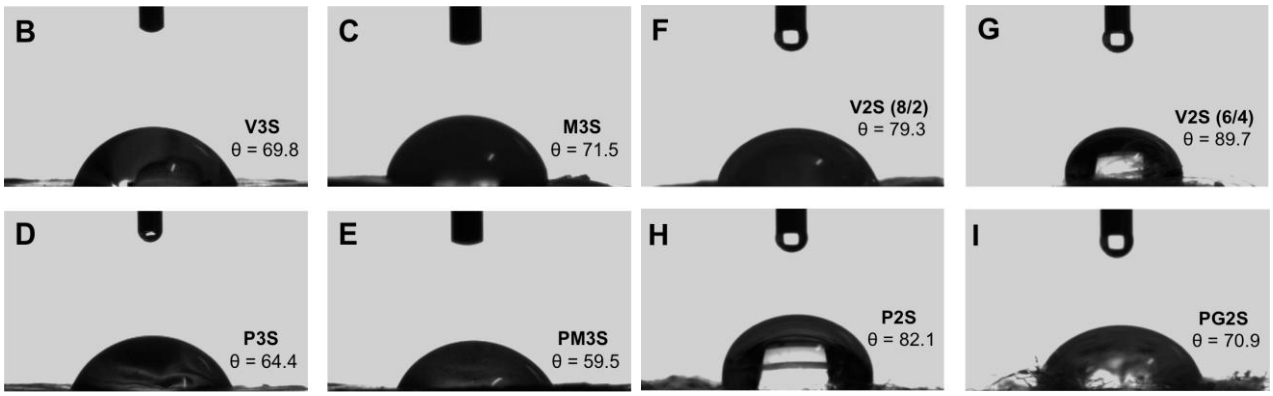

Figure 5. (a) WUC-immersion time curves of all samples in distilled water for 24 hours. (b) Water contact angle of nanofibrous scaffolds (A) and contact angle image of V3S (B), M3S (C), P3S (D),

PM3S (E), V2S (8/2) (F), V2S (6/4) (G), P2S (H), PG2S (I).

3.9. Wettability of nanofibrous scaffolds

Wound healing is more accelerated under moist situations than under dry situations. Traditional wound dressings do not have water retention to minimize dehydration. An ideal wound dressing material should support wound healing by controlling the wetness and humidity and also should be permeable to oxygen and carbon dioxide. Increasing the surface hydrophilicity of hydrophobic materials has been reported to increase cell adhesion and, in particular, cell growth. Nanofibrous scaffolds loaded with PHR ensured adequate moisture and controlled-release, and thereby prevented the wound bed from drying out and promoted recovery. The scaffold matrix also gives some advantages such as preventing continuous wound cleaning and correction. These features offer patients opportunities to deal with improving or reducing pain. Thus, the wettability and hydrophilicity of nanofibrous scaffolds are improved with the presence of PHR and consequently, cell proliferation is promoted.[65]

The thermodynamic balance between interfaces of either a solid, vapour, or liquid determines the surface wettability. Hence, contact angle, θ, describes a quantitative measure of a solid by a liquid. A water contact angle between $0° < \theta < 90°$ indicates that the liquid used wets the surface of solid, conversely $90° < \theta < 180°$ implies that the liquid used does not wet the surface of the solid.[66] The water contact angle of V3S is 69.8° and it increased slightly by adding MET to 71.5°, conversely it decreased by adding PHR to 64.4°, which indicates that MET decreased hydrophilicity of nanofibrous scaffolds; on the other hand, PHR increased hydrophilicity. Moreover, the combination of PHR&MET decreased the contact angle (59.5°) more than PHR only. This indicates that combination of MET and PHR increased hydrophilicity of nanofibrous scaffolds more than their single loaded forms (Figure 5b). The water contact angle of V2S (8/2) is 79.3° and it decreased by adding GB&PHR to 70.9°. On the other hand, the water contact angle of V2S (6/4) is 89.7° and it decreased to 82.1° by adding PHR, which indicates that GB and PHR increased the hydrophilicity of nanofibrous scaffolds. However, it is seen that the 8/2 ratio for PVP/PCL composite fibers is not

favorable to absorb water properly because a high PVP ratio makes nanofibrous scaffolds slightly water-soluble. Conversely, the 6/4 ratio is more suited to absorb water and increasing the hydrophilicity of fibrous scaffolds (Figure 5b).

3.10. In vitro drug release test

In vitro drug release tests were performed for M3S, P3S, PM3S, P2S, and PG2S samples. First, linear standard calibration curves were created for drugs, PHR, MET, and GB (Figure S4a, S4b, and S4c, Supporting Information) and then the encapsulation efficiencies were measured for samples (Figure S4d, Supporting Information). Thereafter, *in vitro* drug release tests were carried out over for 14 days with all drug-loaded samples to investigate the release kinetics of PHR, MET, and GB. The releasing profiles for all samples were performed in phosphate-buffered saline (PBS) at pH 7.4 and 37°C to mimic the physiological conditions of living organisms.

M3S demonstrated sustained drug release for 14 days following a burst release in the first 24 h due to the hydrophobic nature of PCL and crosslinking of nanofibrous scaffolds (Figure 6a). P3S, showed sustained release from the beginning of drug release tests to the end of day 14 except in the first 2 hours and between 2nd and 3rd days in which burst release was observed (Figure 6b). For PM3S, the drug release ratios changed and MET in PM3S released slower than MET in M3S but drug release kinetics did not change and MET showed sustained release following burst release in the first day similar to the M3S sample (Figure 6c). PHR may have caused MET to release slower. In total, 91.8 % of encapsulated MET was released within 14 days from PM3S. On the contrary, MET has caused PHR to release faster in PM3S samples.

P2S showed sustained release from the beginning to the end of the drug release tests. It can be attributed to the higher PCL ratio in the polymer composite (w_{PVP}/w_{PCL}=6/4). More PHR was released from PNM (93.2%) compared with GPNM at the end of 14 days (Figure 6d).

On the other hand, PG2S showed burst release on the first day due to the higher PVP ratio in the polymer composite (w_{PVP}/w_{PCL}=8/2) - GPNM. 52.7% of total GB and 57.4% of total PHR in the GPNM samples were released in first day. The samples demonstrated sustained release till the last

day of the drug release tests (Figure 6e). All GB in the nanofibrous scaffolds was released in 14 days, however 83.6% of the total PHR was released in 14 days. Therefore, according to drug release test results, the combination of two medicines accelerated the release of PHR on the first day and decelerated later on. Moreover, *in vivo* diabetic wound healing tests were performed on rats in order to investigate the biological effects of drug release kinetics for all samples. As a result, all samples exhibited a controlled release for 14 days and reached a peak on the last day as discussed below.

According to the *in vitro* drug release profiles of nanofibrous scaffolds in our study, drug release in all samples reached approximately 50% in the first 3 days. The first burst of drug release occurred due to some drug molecules being located on the surface of scaffolds. Drug release was controlled just by diffusion and polymer degradation after the first burst.[65] Therefore, MET, PHR, and GB are released from scaffolds in a relatively controlled manner. In general, biodegradable drug release fibers released a high concentration of loaded drugs and were functionally active during the animal experiments for the treatment of diabetic wounds.

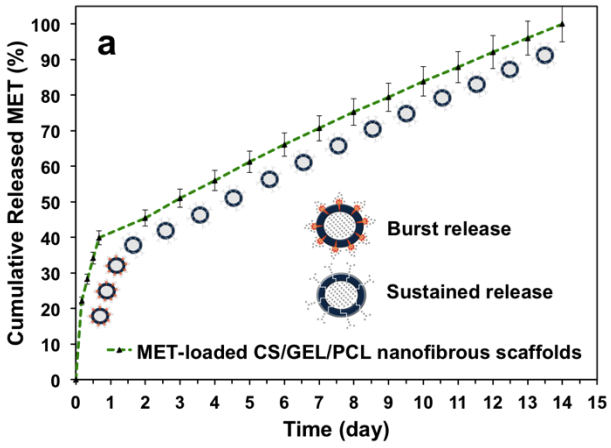

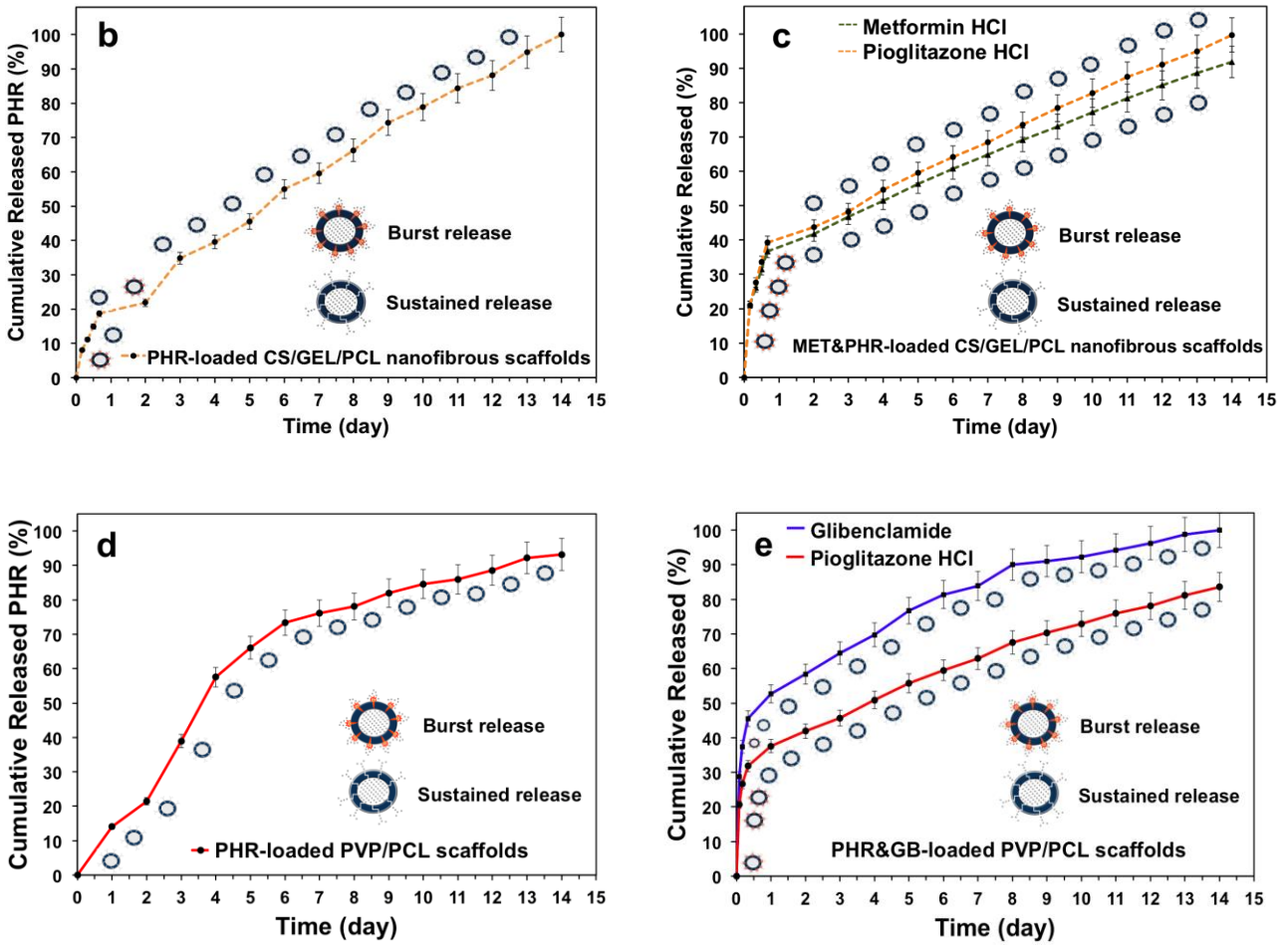

Figure 6. *In vitro* drug release profiles of nanofibrous scaffolds: (a) MET release profile of M3S, (b) PHR release profile of P3S, (c) MET and PHR release profile of PM3S, (d) PHR release profile of P2S, and (e) GB and PHR release profile of PG2S. The drug release experiments were repeated three times for each sample and the average was taken. The errors were below 5%.

3.11. In vitro drug release kinetics

The release kinetics of MET, PHR, and GB were investigated by Korsmeyer-Peppas, zero order, first order, Higuchi, Hixon-Crowell models. The obtained kinetic constants and regression coefficients (R^2) of all nanofibrous scaffols were given in Table 1. The Higuchi model has better agreement with higher R^2 values for M3S (Figure S5), P3S (Figure S6), and PM3S (Figure S7), which were produced by electrospinning; whereas, the first order model has better agreement with higher R^2 values for P2S (Figure S8) and PG2S (Figure S9), which were produced by pressurized gyration. Kinetic modelling data of MET, PHR, and GB release from all samples incubated in

dynamic conditions in PBS (pH 7.4) at 37ºC are given in Supporting Information, Figure S5-S9.

Moreover, the value of n describes the mechanism of drug release from a polymeric system in the Korsmeyer–Peppas model. For a cylindrical system, 0.45 ≥ n corresponds to a Fickian diffusion and 0.45 < n < 1 refers the non-Fickian diffusion [67]. All the n values of nanofiber samples are between 0.45 and 1, which is showing that all drugs were released from nanofibrous scaffolds through the non-Fickian diffusion mechanism.

Table 1. Comparison of drug release data generated using different models for nanofibrous scaffolds used in this work

		Korsmeyer-Peppas		**Zero Order**		**First Order**		**Higuchi**		**Hixon-Crowell**	
Sample		R^2	n	R^2	K_0	R^2	K_1	R^2	K_h	R^2	K_{hc}
M3S		0,7694	0,5384	0,9137	0,2326	0,8517	-0,0041	0,9775	4,6821	0,8820	0,0092
P3S		0,9523	0,6652	0,9864	0,2802	0,8123	-0,0041	0,9763	5,4250	0,8708	0,0097
PM3S	MET	0,7719	0,5293	0,9152	0,2139	0,9623	-0,0026	0,9772	4,3013	0,9742	0,0064
	PHR	0,7748	0,5395	0,9215	0,2326	0,7435	-0,0043	0,9760	4,6597	0,9290	0,0084
P2S		0,9809	0,7990	0,8545	0,2623	0,9872	-0,0034	0,9494	5,7183	0,9623	0,0081
PG2S	GB	0,6390	0,4589	0,7997	0,2171	0,9501	-0,0049	0,9354	4,4952	0,9439	0,0100
	PHR	0,6945	0,4576	0,8819	0,1903	0,9790	-0,0020	0,9681	3,8171	0,9605	0,0051

3.12. Evaluation of cell viability

A cytotoxicity test should be performed via investigation of cell viability to determine the potential of a nanofibrous scaffold as a wound dressing. Cytotoxicity assay results showed that none of the scaffolds have cytotoxic effect on healthy cells (Figure 7a). Hence, these fibers can be safely used for animal tests and the biocompatibility test exhibited that all samples have good cytocompatibility and thus these samples can be used in further studies on biomedical applications.

The confluent cells were viewed by SEM and it was observed that the cell clusters on all samples are properly proliferating. Therefore, it has been confirmed that the nanofibrous scaffolds do not have cytotoxic effects on mouse fibroblast cells and, also, they create a suitable area for the growth of fibroblast cells (Figure 7b-h). Only M3S increased cell survival among drug-loaded nanofibrous scaffolds but there is no significant difference compared to the control group. MTT test results of nanofibrous scaffolds are compatible with SEM images.

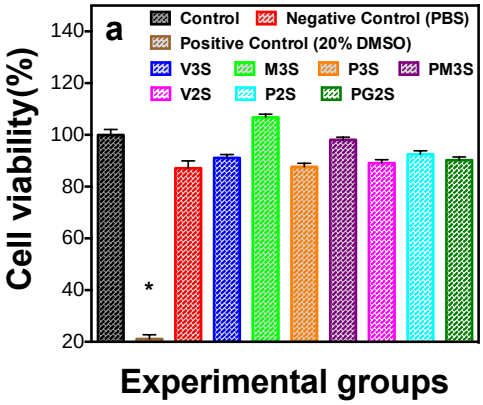

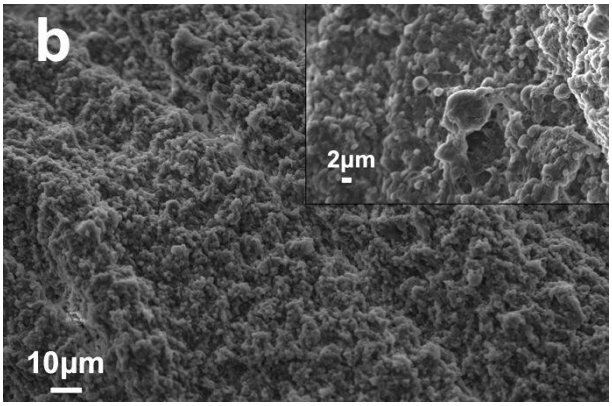

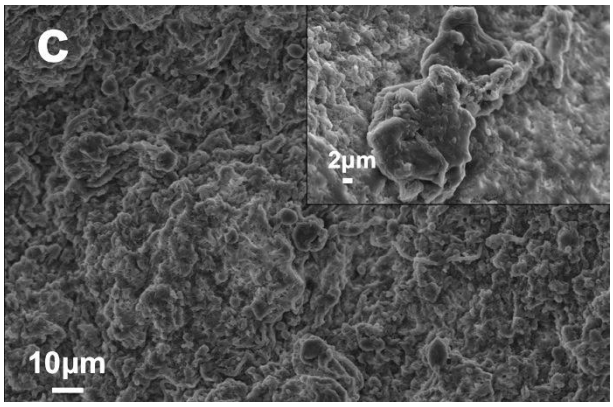

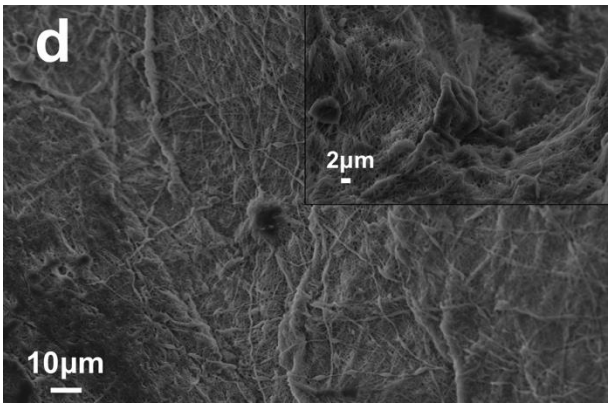

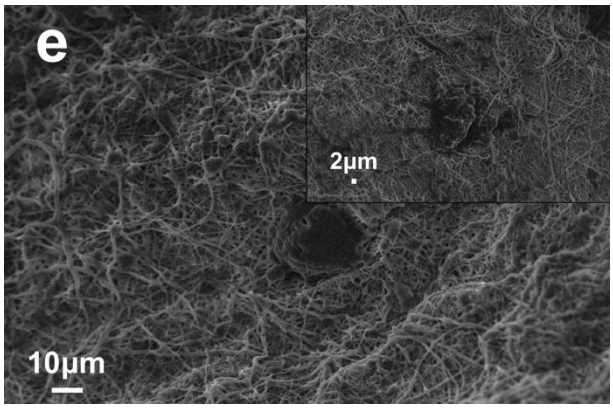

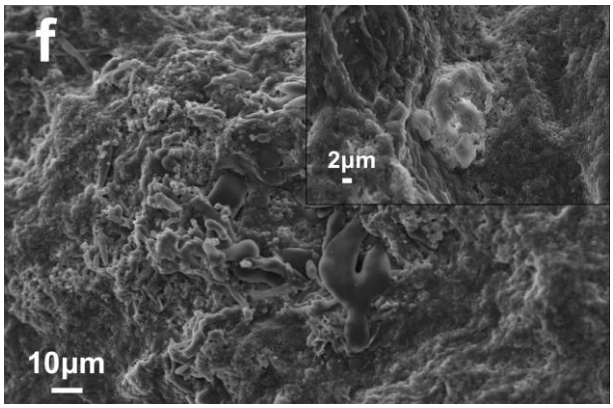

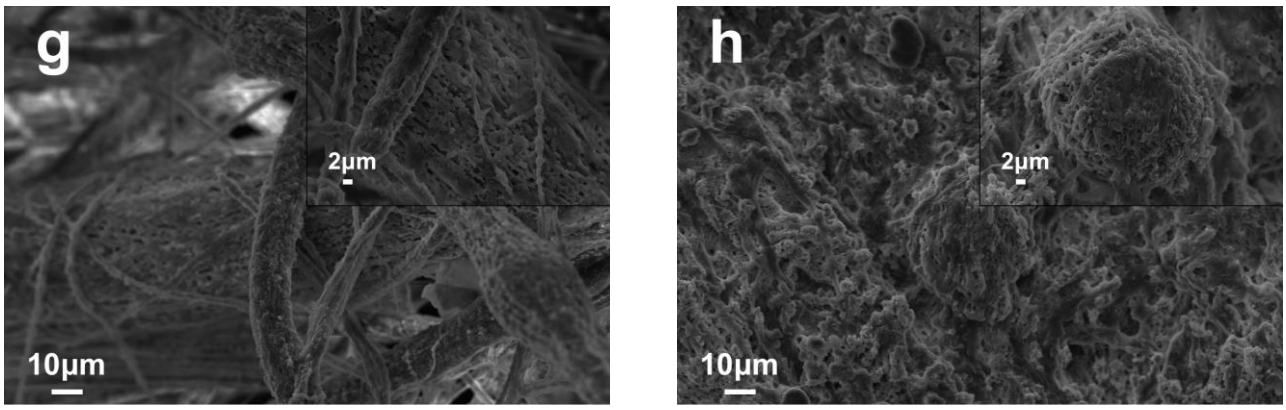

Figure 7. (a) L929 (mouse fibroblast) cell viability of all samples. The data are presented as mean ± standard error of the mean. *p<0.05 versus the control group. SEM images of proliferated cells on (b) V3S, (c) M3S, (d) P3S, (e) PM3S, (f) V2S, (g) P2S, and (h) PG2S.

3.13. In vivo wound healing tests

The STZ-induced wound model was preferred in our study due to similar pathologies with chronic wounds in many studies.[e.g. 68] These have shown the persistent infiltration of inflammatory cells in to wound areas, thus limiting the closure of diabetic wounds.[69] The evaluation of diabetic wound healing ability is given in Figures 8a and 8b, in terms of appearance of the healing wound and change in wound area after treatments, respectively. During the wound healing process, wound sizes of the diabetic animals were photographed and measured.

Figure 8a presents wound images which belong to an animal from each group [control group (A), V3S group (B), M3S group (C), P3S group (D), PM3S group (E), V2S group (F), P2S group (G), and PG2S (H)], on days 0, 3, 7, 10, and 14 following wound creation. On day 3, the wound closure of the treated rats was mildly visible compared to untreated rats. The wound closure in the treatment groups with drug-loaded scaffolds on days 7 and 10 was apparently faster than untreated groups and the treatment groups with pure scaffolds. Finally, on day 14, wound healing was almost complete in groups C, D, E, G, and H compared to A, B, and F groups. Moreover, group E and H visibly demonstrated a quicker healing process between day 7 and 14.

Figure 8b indicates the changes in wound closure calculations on 3^{rd}, 7^{th}, 10^{th}, 12^{th} and 14^{th} days

between all experimental groups. On the 7th day, the mean values of wounded area in rats treated with V3S, M3S, P3S, PM3S, V2S, P2S, and PG2S decreased to 35.8 ± 2.3%, 29.7 ± 2.9%, 29.6 ± 5.2%, 23.7 ± 3.4%, 50.4 ± 1.5%, 38.9 ± 1.7%, and 29.7 ± 2.3% respectively, when in control animals it decreased to 52.7 ± 1.7%. According to these results, PM3S caused the best improvement ($p<0.001$) on days 7 and 10 compared to the control group.

When appearance of healing wounds and change in wounds area were evaluated, there are significant therapeutic effects seen in V3S group. This may be due to some of the characteristics of CS and GEL. CS is a biodegradable polysaccharide obtainable by deacetylation of chitin. In addition to its biocompatibility, biodegradability and hemostasis ability, CS possesses antibacterial and antifungal activity [70]. GEL maintains molecular signals that can control cell behavior and absorbs the wound exudate [17, 18]. These advantages of CS and GEL improved wound healing and decreased pro-inflammatory cytokine levels in the tissues compared to the control group. Nanofibers are ideal for wound healing because their dimensions are similar to the components of the native extracellular matrix and mimics its fibrillar structure, providing essential cues for cellular organization and survival function [71]. Therefore, V2S has diabetic wound healing effect although it contains no drugs. V3S showed better improvement ($p<0.001$) than V2S on day 7 and it can be clearly seen that CS/GEL/PCL composite has better wound healing properties than the PVP/PCL composite. This can be attributed individually proven wound healing effects of chitosan and gelatin.[72] On the other hand, all drug-loaded nanofibrous scaffolds showed better improvement than their virgin forms. This suggests that PHR, MET and GB are effective in promoting wound healing in hyperglycemic rats but the combination of these drugs are even more effective. On days 10 and 12, there was a significant difference in all treatment groups except of V2S compared to the control group. On day 14, the last day of the animal test, wounds were almost closed in all groups and there is no statistically significant difference between the study groups. From details on the last day, the means of wounded area with control, V3S, M3S, P3S, PM3S, V2S, P2S, and PG2S groups decreased to 10.2 ± 0.6%, 6.7 ± 0.6%, 3.5 ± 0.7%, 2.6 ± 0.6%, 2.6 ± 0.7%, 8.5 ± 0.6%, 5.4 ± 1.1%,

1.7 ± 0.1%, respectively.

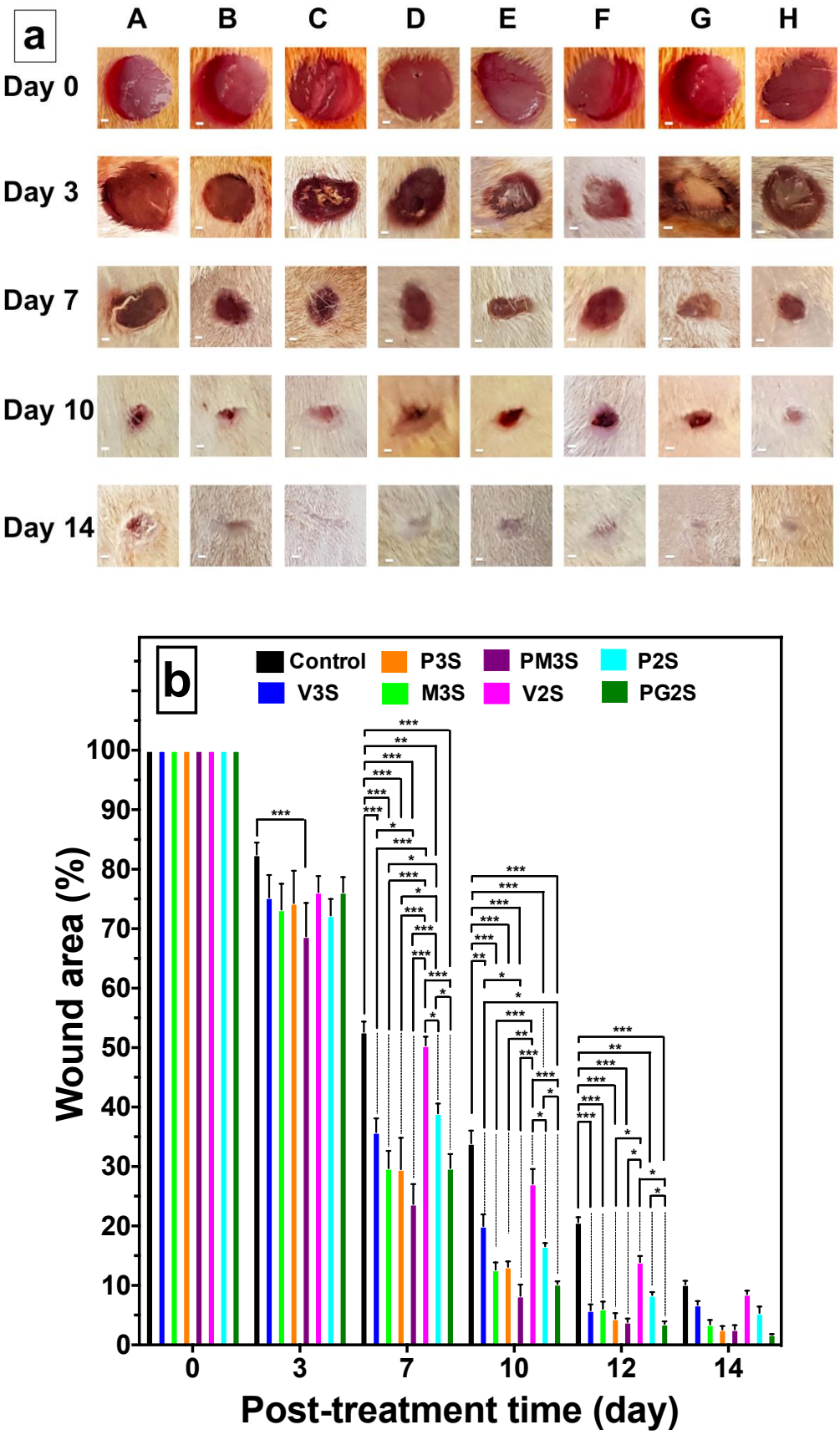

Figure 8. (a) Photographs of wounds and (b) wound area values on various days after surgical

incision: (A) control group, (B) V3S group, (C) M3S group, (D) P3S group, (E) PM3S group, (F) V2S group, (G) P2S group, and (H) PG2S. Scale bar: 1 mm. The data is presented as mean ± standard error of the mean. *p < 0.05, **p < 0.01, ***p < 0.001.

3.14. Histological evaluation

The wounded tissues stained with H&E (Figure 9a) and Gomori's trichrome (Figure 9b) were examined and scored histopathologically at days 3, 7, and 14 (Table S2, Supporting Information). On day 3, all CS/GEL/PCL groups showed damage of the dermis with epidermal detachment, scab formation with necrotic tissue remnants, vasocongestion, edema and inflammatory cell formation (Figure 9a). On the other hand, the skin wound samples revealed evident vasocongestion and neutrophil infiltration beside hemorrhage, edema and exudate at day 3 in all PVP/PCL groups (Figure 9a). The inflammatory cell infiltration in the skin samples on day 3 is shown clearly with higher magnification images taken from the H&E stained skin samples in Figure S10, Supporting Information. On day 7, beginning of epithelialization in the drug loaded CS/GEL/PCL nanofibrous scaffold groups was observed with granulation tissue formation, especially the PM3S group demonstrated better improvement compared to M3S and P3S groups. Thick scabbing was still observed especially in the control and V3S groups with granulation tissue in the dermis. Although present in all groups, the PM3S group showed less inflammatory cell infiltration and edema compared to other groups. P2S and PG2S groups showed limited wound area with few thin collagen fibers in the deep dermis and also slightly decreased edema compared to control and V2S groups (Figure 9b). Ongoing hemorrhage with neutrophil infiltration was still seen at day 7 in control and V2S groups with increased fibroblasts, however the collagen fibers were thicker and better organized in the dermis of P2S and PG2S group rats. Few inflammatory cells and little hemorrhage were observed beneath the scab and poorly regenerated epidermis was a feature in all groups. On day 14, experimental groups showed more developed epithelialization; however, in the drug loaded CS/GEL/PCL nanofibrous scaffold groups densely packed collagen fibers in the dermis were more organized (Figure 9b). Better regeneration of the dermis and epidermis in the M3S and PM3S

groups with less inflammatory cell infiltration and edema were observed compared to control and V3S groups. However, the formation of the hair follicles was observed only in the PM3S group. For PVP/PCL groups, on day 14, the P2S and PG2S groups showed better organized epidermis and dermis in contrast to the granulation tissue composed of thin and unclear collagen fibers in the control and V2S groups.

Wound length measurements were given in Figure 9c. There was no significant difference between groups on day 3, however all drug-loaded nanofibrous scaffold groups considerably decreased wound length on day 7 and 14 compared to control and virgin nanofibrous scaffold groups. PM3S group showed significantly decreased ($p<0.05$) wound length compared to M3S and P3S groups on days 7 and 14. Similar results were observed for PG2S group, it had reduced wound length compared to the V2S group on days 7 and 14 ($p<0.05$).

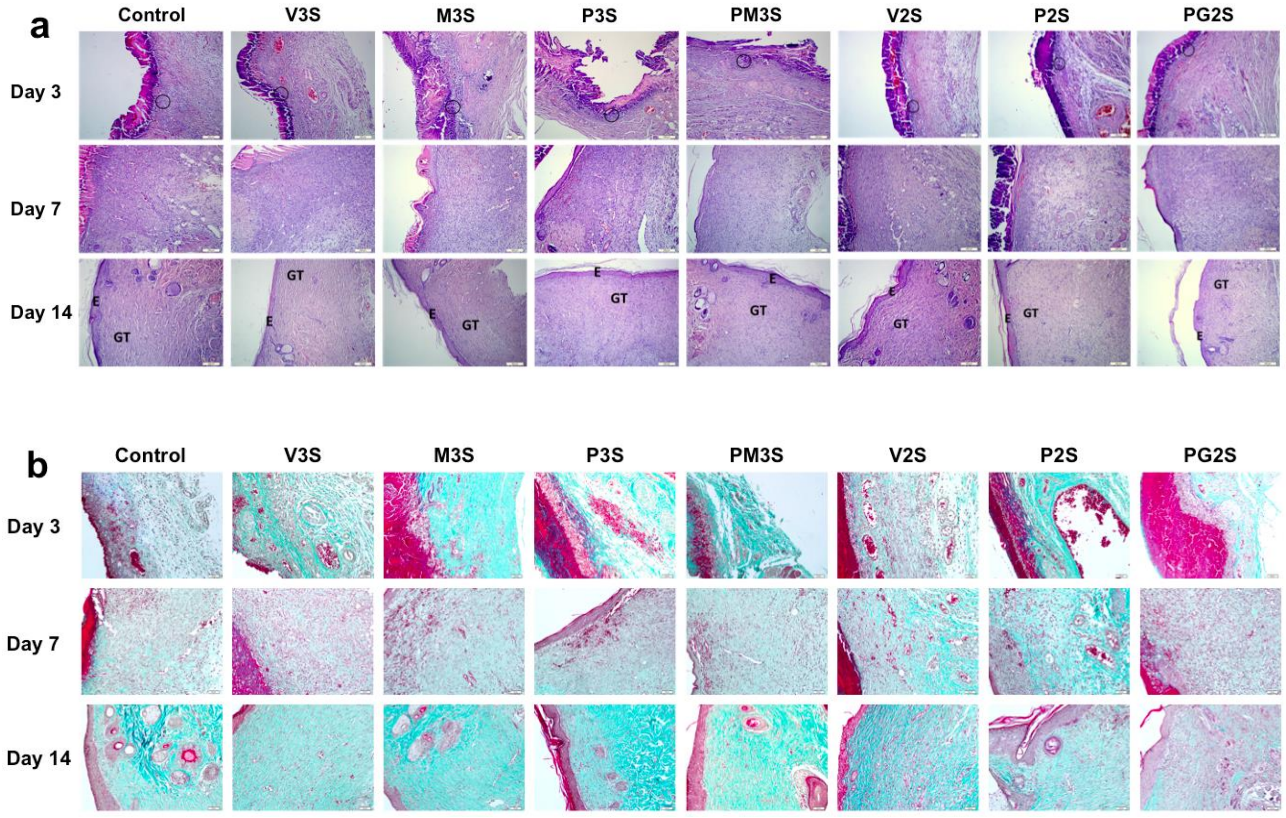

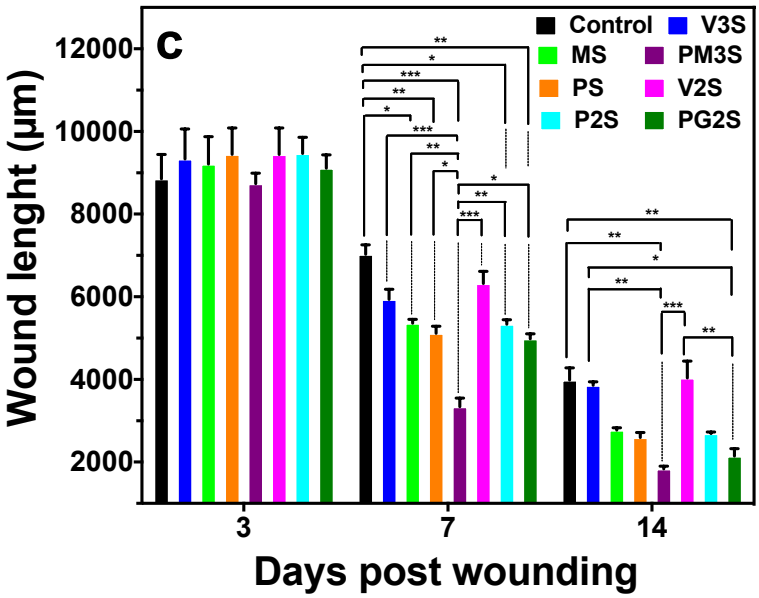

Figure 9. Histopathological evaluations. Representative microscopic images of skin wound sections from control, V3S, M3S, P3S, PM3S, V2S, P2S, and PG2S groups on various days. (a) Hematoxylin and eosin staining. The circles indicate inflammatory cell infiltration. GT: Granulation tissue. E: Epithelium. Scale bars: 200 µm. (b) Gomori's trichrome stain. Blue staining shows collagen fibers. Scale bars: 50 µm. (c) The change in wound length for all groups on various days. The values were calculated as the mean ± standard error mean (n=6). ***p< 0.001, **p< 0.01, *p< 0.05.

3.15. Biochemical evaluation

TNF-α, IL-6, and IL-1β, which are pro-inflammatory cytokines responsible for the migration of immune cells, participate in the inflammatory phase. NF-κB is an essential regulator for the control of many pro-inflammatory genes, such as TNF-α and IL-1β. Interleukin 10 (IL-10) is an anti-inflammatory cytokine and limits the host immune response to pathogens, hence it prevents the host from damage and maintains normal tissue homeostasis. Previous studies have reported that the level of TNF-α, IL-6, IL-1β, and NF-κB are higher and on the contrary, IL-10 levels are lower in chronic wounds [73-76]. ELISA kits were utilized according to manufacturer's instructions to measure the concentrations of all these cytokines in the wound areas on day 14 (Figure 10). Expression level of TNF-α, IL-6, IL-1β, and NF-κB was significantly lower ($p<0.005$) in all treated rats compared to

untreated rats. Moreover, the level of TNF-α, IL-6, IL-1β, and NF-κB in the drug-loaded nanofibrous scaffold groups was significantly lower than their respective virgin groups. M3S group showed better anti-inflammatory effects than P3S group but there is no significant difference between them in TNF-α, IL-6, IL-1β, and NF-κB levels, only IL-10 levels of M3S group is significantly higher ($p<0.05$) than the P3S group. The highest decrease of TNF-α, IL-6, IL-1β, and NF-κB levels and the highest increase of IL-10 levels were seen in PM3S followed by the PG2S groups. As a result, it was shown that TNF-α, IL-6, IL-1β, and NF-κB levels were significantly higher as detected with biochemical analysis at the end of 14th day and in accordance with the histological findings, which showed more neutrophil infiltration and edema in diabetic animals.

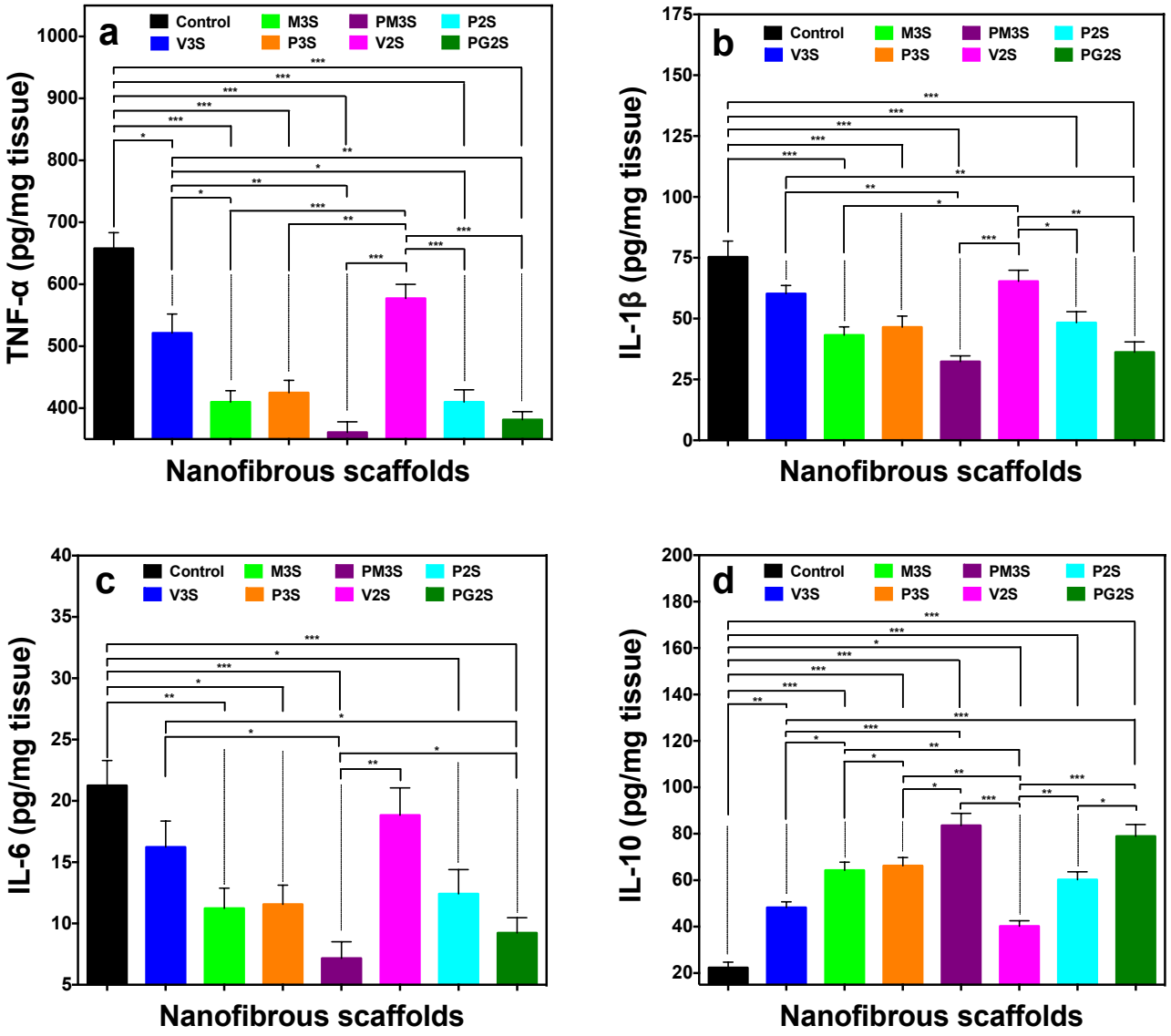

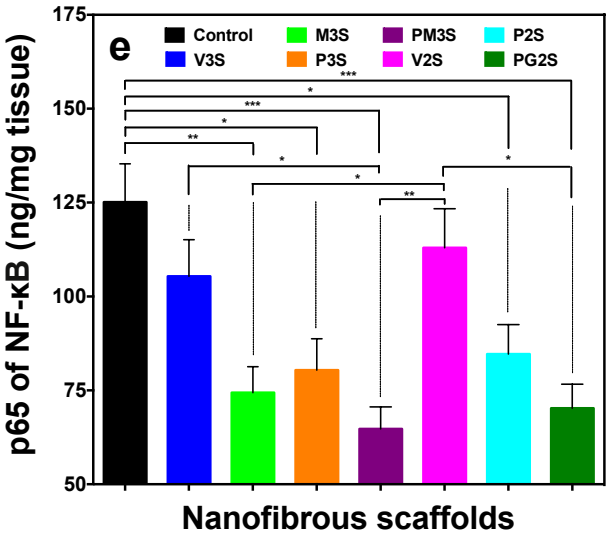

Figure 10. The level of TNF-α, IL-1β, IL-6, IL-10, p65 of NF-κB in the wounded area on day 14. The data is presented as mean ± standard error of the mean. *p < 0.05, **p < 0.01, ***p < 0.001.

A complete relief or improvement was not provided by current treatments and there are some disadvantages for each treatment in clinical practice such as the presence of side effects like hypoglycemia, lactic acidosis, peripheral edema and the increased risk for congestive heart failure and gastrointestinal symptoms.[77] Many treatments such as artificial skin, platelet-rich plasma or local stem cell injection produced by tissue engineering are currently under development. Diabetic wound healing therapy still needs further research and therapeutic indexing. However, the possibility of a drug that targets the AMPK, PPAR-γ, and K_{ATP} channel can give new hope. Due to the complicated pathological mechanisms of diabetic wounds, combination of these drugs can provide a therapeutic advantage for patients with diabetic wounds.[78] Therefore, in our study, a AMPK activator, and K_{ATP} channel blocker were chosen to combine with PPAR-γ agonist and loaded into CS/GEL/PCL and PVP/PCL nanofibrous scaffolds to provide an effective treatment.

AMPK activation causes blocking of advanced glycation end-product (AGE) signaling; suppressing receptor advanced glycation end-products (RAGE) expression; inhibiting NF-κB, TNF-α and IL-6; increasing vascular endothelial growth factor, von Willebrand factor expression and angiogenesis.[79] As a result, it is thought that AMPK activation may be beneficial in diabetic wound treatment by RAGE/AGE signaling blockade, angiogenesis, anti-inflammation, anti-

oxidation, promotion of proliferation and migration of fibroblasts and keratinocyte, and protection against vascular damage.[78]

Pioglitazone binds specific DNA sequences and demonstrates strong anti-inflammatory activity by inhibiting pro-inflammatory gene transcription or by activating pro-resolving genes. [80] PPAR-γ activation has been shown to reduce the expression of pro-inflammatory proteins and genes, including TNF-α.[81] Furthermore, PPAR-γ activity inhibits inflammation by increasing M2 cells and decreasing M1 cells. [82] According to our results in the present study, when PHR is used alone or in combination with MET or GB, accelerated diabetic wound closure and improved biochemical and histological scenarios result. The combinations gave rise to accelerated wound healing and showed higher anti-inflammatory effects.

The wound healing effect of GB is to inhibit the expression of RIP140 by increasing intracellular Ca^{++} flow.[83] RIP140, a nuclear receptor coregulator, is a NF-κB cofactor that increases M1 polarization and a STAT6 inhibitor that suppresses M2 polarization in macrophages.[84] To control the level of RIP140 protein is a treatment option to eliminate inflammation. Studies aiming to alter RIP140 protein levels in diseases associated with chronic inflammation have concluded that GB may be a potential therapeutic agent.[83, 85, 86] According to the results of a wound study with high-fat diet fed animals, the healing effect of the topical application of GB has been associated with the anti-inflammatory potential. Moreover, treatment with GB reduced RIP140 protein level in macrophages and increased M2 level and decreased M1 level.[83] These results were confirmed in our study and GB has strengthened the anti-inflammatory effect of PG2S compared to P2S.

4. Conclusions

The new strategies for combination therapy with PPAR-γ agonist may provide a therapeutic advantage for patients with diabetic wounds. Therefore, in our study, PPAR-γ agonist was combined with AMPK activator and K_{ATP} channel blocker successfully loaded into CS/GEL/PCL and PVP/PCL nanofibrous scaffolds to provide an effective treatment. Moreover, AMPK activator and PPAR-γ agonist were separately loaded into nanofibrous scaffolds to compare the diabetic

wound healing effect with combination therapy. It was clearly shown that the combination therapy increased the wettability and hydrophilicity of scaffolds, which potentially promotes cell proliferation. It demonstrated sustained drug release over 14 days and it was functionally active during the animal experiments. The scaffolds have proper tensile strength and suitable cytocompatibility on L929 (mouse fibroblast) cells and created a suitable area for the proliferation of fibroblast cells, and it can safely be applied on wound sites without risk of melting. Therefore, PM3S and PG2S accelerated diabetic wound healing in type-1 diabetic rats more significantly and better organized densely packed collagen fibers in the dermis. These also showed better regeneration of the dermis and epidermis with less inflammatory cell infiltration and edema. The formation of the hair follicles started only in the PM3S group in 14 days and the lowest pro-inflammatory cytokine levels were observed in the PM3S group compared to the others. The results demonstrate that topical administration of the combination of AMPK activator and PPAR-γ agonist in CS/GEL/PCL nanofibrous scaffolds offer significant potential for the treatment of diabetic wounds with high bioavailability and fewer systemic side effects.

Acknowledgments

Dr. Muhammet E. Cam was supported by a TUBITAK 2219 Research Programme Grant (Scientific and Technological Research Council of Turkey-TUBITAK, Grant No. 1059B191800800) and thanks UCL Mechanical Engineering for hosting his post-doctoral research in the UK. Hussain Alenezi wishes to thank PAAET-Kuwait for sponsoring his Ph.D. research (Grant No. 278010301647). The authors are grateful to the UK Engineering & Physical Sciences Research Council (EPSRC) for funding pressurized gyration forming research at University College London (Grants EP/S016872/1 and EP/N034228/1).

Supporting Information

The Supporting Information includes the results and discussion for the physical properties of solutions, process conditions, fiber diameter distribution of nanofibrous scaffolds, calibration curves and encapsulation efficiency for *in vitro* drug release studies, and the parameters for histological scoring. The following files are available free of charge: Figure S1. The production yield of all PVP/PCL nanofibrous scaffold samples, comparing pressurized gyration and electrospinning. Figure S2. Fiber diameter distributions of virgin CS/GEL/PCL fibrous scaffolds. Figure S3. Fiber diameter distributions of PVP/PCL (12%, w/v) nanofibrous scaffolds. Figure S4. Calibration curves and encapsulation efficiency for *in vitro* drug release studies. Figure S5. Kinetic model elaboration of MET release from M3S. Figure S6. Kinetic model elaboration of PHR release from P3S. Figure S7. Kinetic model elaboration of MET and PHR release from PM3S. Figure S8. Kinetic model elaboration of PHR release from P2S. Figure S9. Kinetic model elaboration of GB and PHR release from PG2S. Figure S10. Representative photomicrographs of skin tissues in the experimental rat groups on day 3. Table S1. Parameters used to generate the samples. Table S2. Histopathological scoring on days 3, 7, and 14.

Author Contributions

The manuscript was written by collecting contributions from all authors. All authors have given approval to the final version of the manuscript.

Conflicts of Interest

The authors declare no conflict of interest.

References

[1] M.E. Cam, A.N. Hazar-Yavuz, S. Yildiz, B. Ertas, B. Ayaz Adakul, T. Taskin, S. Alan, L. Kabasakal, The methanolic extract of Thymus praecox subsp. skorpilii var. skorpilii restores glucose homeostasis, ameliorates insulin resistance and improves pancreatic beta-cell function on streptozotocin/nicotinamide-induced type 2 diabetic rats, J. Ethnopharmacol. 231 (2019) 29-38.

[2] A. American Diabetes, Diagnosis and classification of diabetes mellitus, Diabetes Care 32 Suppl 1 (2009) S62-S67.

[3] M.E. Cam, S. Yildiz, B. Ertas, A. Eda Acar, T. Taskin, L. Kabasakal, Antidiabetic effects of Salvia triloba and Thymus praecox subsp. Skorpilii var. skorpilii in a rat model of streptozotocin/nicotinamide-induced diabetes, Mar. Pharm. J. 21 (2017) 818-827.

[4] S. Wild, G. Roglic, A. Green, R. Sicree, H. King, Global prevalence of diabetes: estimates for the year 2000 and projections for 2030, Diabetes Care 27 (2004) 1047-1053.

[5] P. Mostafalu, G. Kiaee, G. Giatsidis, A. Khalilpour, M. Nabavinia, M.R. Dokmeci, S. Sonkusale, D.P. Orgill, A. Tamayol, A. Khademhosseini, A Textile Dressing for Temporal and Dosage Controlled Drug Delivery, Adv. Funct. Mater. 27 (2017) 1702399.

[6] E. Ilhan, S. Cesur, E. Guler, F. Topal, D. Albayrak, M.M. Guncu, M.E. Cam, T. Taskin, H.T. Sasmazel, B. Aksu, F.N. Oktar, O. Gunduz, Development of Satureja cuneifolia-loaded sodium alginate/polyethylene glycol scaffolds produced by 3D-printing technology as a diabetic wound dressing material, Int. J. Biol. Macromol. 161 (2020) 1040-1054.

[7] G. Han, R. Ceilley, Chronic Wound Healing: A Review of Current Management and Treatments, Adv. Ther. 34 (2017) 599-610.

[8] J. Xiao, S. Chen, J. Yi, H.F. Zhang, G.A. Ameer, A Cooperative Copper Metal–Organic Framework-Hydrogel System Improves Wound Healing in Diabetes, Adv. Funct. Mater. 27 (2017) 1604872.

[9] C. Qing, The molecular biology in wound healing & non-healing wound, Chin. J. Traumatol. 20 (2017) 189-193.

[10] V. Coger, N. Million, C. Rehbock, B. Sures, M. Nachev, S. Barcikowski, N. Wistuba, S. Strauss, P.M. Vogt, Tissue Concentrations of Zinc, Iron, Copper, and Magnesium During the Phases of Full Thickness Wound Healing in a Rodent Model, Biological trace element research (2018).

[11] B. Mordorski, J. Rosen, A. Friedman, Nanotechnology as an innovative approach for accelerating wound healing in diabetes, Future Medicine 5 (2015) 329-332.

[12] T. Taskin, M.E. Cam, D. Taskin, E. Rayaman, In vitro and In vivo biological activities and phenolic characterization of Thymus praecox subsp. skorpilii var. skorpilii, J. Food Meas. Charact. 13 (2018) 536-544.

[13] X. Wang, M.K. Sng, S. Foo, H.C. Chong, W.L. Lee, M.B. Tang, K.W. Ng, B. Luo, C. Choong, M.T. Wong, B.M. Tong, S. Chiba, S.C. Loo, P. Zhu, N.S. Tan, Early controlled release of peroxisome proliferator-activated receptor beta/delta agonist GW501516 improves diabetic wound healing through redox modulation of wound microenvironment, J. Control. Release 197 (2015) 138-147.

[14] A.M. Rasik, A. Shukla, Antioxidant status in delayed healing type of wounds, Int. J. Exp. Pathol. 81 (2000) 257-263.

[15] K.A. Rieger, N.P. Birch, J.D. Schiffman, Designing electrospun nanofiber mats to promote wound healing – a review, J. Mater. Chem. B 1 (2013) 4531-4541.

[16] M.J. Callaghan, D.J. Ceradini, G.C. Gurtner, Hyperglycemia-induced reactive oxygen species and impaired endothelial progenitor cell function, Antioxid. Redox Signal. 7 (2005) 1476-1482.

[17] S. Gnavi, B.E. Fornasari, C. Tonda-Turo, R. Laurano, M. Zanetti, G. Ciardelli, S. Geuna, The Effect of Electrospun Gelatin Fibers Alignment on Schwann Cell and Axon Behavior and Organization in the Perspective of Artificial Nerve Design, Int. J. Mol. Sci. 16 (2015) 12925-12942.

[18] S.H. Lee, Y. Lee, Y.W. Chun, S.W. Crowder, P.P. Young, K.D. Park, H.-J. Sung, In Situ Crosslinkable Gelatin Hydrogels for Vasculogenic Induction and Delivery of Mesenchymal Stem Cells, Adv. Funct. Mater. 24 (2014) 6771-6781.

[19] N. Monteiro, M. Martins, A. Martins, N.A. Fonseca, J.N. Moreira, R.L. Reis, N.M. Neves, Antibacterial activity of chitosan nanofiber meshes with liposomes immobilized releasing gentamicin, Acta Biomater. 18 (2015) 196-205.

[20] B.L. Farrugia, Y. Mi, H.N. Kim, J.M. Whitelock, S.M. Baker, W.P. Wiesmann, Z. Li, P. Maitz, M.S. Lord, Chitosan-Based Heparan Sulfate Mimetics Promote Epidermal Formation in a Human Organotypic Skin Model, Adv. Funct. Mater. 28 (2018) 1802818.

[21] Z.-C. Yao, Y. Gao, M.-W. Chang, Z. Ahmad, J.-S. Li, Regulating poly-caprolactone fiber characteristics in-situ during one-step coaxial electrospinning via enveloping liquids, Materials Letters 183 (2016) 202-206.

[22] H.L. Zeng, C. Gao, D.Y. Yan, Poly(ϵ-caprolactone)-Functionalized Carbon Nanotubes and Their Biodegradation Properties, Adv. Funct. Mater. 16 (2006) 812-818.

[23] Z. Zhu, C. Xie, Q. Liu, X. Zhen, X. Zheng, W. Wu, R. Li, Y. Ding, X. Jiang, B. Liu, The effect of hydrophilic chain length and iRGD on drug delivery from poly(ε-caprolactone)-poly(N-vinylpyrrolidone) nanoparticles, Biomaterials 32 (2011) 9525-9535.

[24] J.C. Wang, H. Zheng, M.W. Chang, Z. Ahmad, J.S. Li, Preparation of active 3D film patches via aligned fiber electrohydrodynamic (EHD) printing, Sci. Rep. 7 (2017) 43924.

[25] J.C. Dumville, B.A. Lipsky, C. Hoey, M. Cruciani, M. Fiscon, J. Xia, Topical antimicrobial agents for treating foot ulcers in people with diabetes, Cochrane Database Syst. Rev. 6 (2017) Cd011038.

[26] V. Kothari, J.A. Galdo, S.T. Mathews, Hypoglycemic agents and potential anti-inflammatory activity, J. Inflamm. Res. 9 (2016) 27-38.

[27] M.E. Cam, M. Crabbe-Mann, H. Alenezi, A.N. Hazar-Yavuz, B. Ertas, C. Ekentok, G.S. Ozcan, F. Topal, E. Guler, Y. Yazir, M. Parhizkar, M. Edirisinghe, The comparision of glybenclamide and metformin-loaded bacterial cellulose/gelatin nanofibres produced by a portable electrohydrodynamic gun for diabetic wound healing, Eur. Polym. J. 134 (2020) 109844.

[28] M.E. Cam, S. Yildiz, H. Alenezi, S. Cesur, G.S. Ozcan, G. Erdemir, U. Edirisinghe, D. Akakin, D.S. Kuruca, L. Kabasakal, O. Gunduz, M. Edirisinghe, Evaluation of burst release and sustained release of pioglitazone-loaded fibrous mats on diabetic wound healing: an in vitro and in vivo comparison study, J. R. Soc. Interface 17 (2020) 20190712.

[29] K. Isoda, J.L. Young, A. Zirlik, L.A. MacFarlane, N. Tsuboi, N. Gerdes, U. Schonbeck, P. Libby, Metformin inhibits proinflammatory responses and nuclear factor-kappaB in human vascular wall cells, Arter. Thromb. Vasc. Biol. 26 (2006) 611-617.

[30] J.J. Salazar, W.J. Ennis, T.J. Koh, Diabetes medications: Impact on inflammation and wound healing, J. Diabetes Complicat. 30 (2016) 746-752.

[31] S.R. Gomes, G. Rodrigues, G.G. Martins, M.A. Roberto, M. Mafra, C.M. Henriques, J.C. Silva, In vitro and in vivo evaluation of electrospun nanofibers of PCL, chitosan and gelatin: a comparative study, Mater. Sci. Eng. C Mater. Biol. Appl. 46 (2015) 348-358.

[32] B. Dhandayuthapani, U.M. Krishnan, S. Sethuraman, Fabrication and characterization of chitosan-gelatin blend nanofibers for skin tissue engineering, J. Biomed. Mater. Res. B 94 (2010) 264-272.

[33] N. Amiri, Z. Rozbeh, T. Afrough, S.A. Sajadi Tabassi, A. Moradi, J. Movaffagh, Optimization of Chitosan-Gelatin Nanofibers Production: Investigating the Effect of Solution Properties and Working Parameters on Fibers Diameter, BioNanoScience 8 (2018) 778-789.

[34] S. Habibi, K. Hajinasrollah, Electrospinning of Nanofibers Based on Chitosan/Gelatin Blend for Antibacterial Uses, Russ. J. Appl. Chem. 91 (2018) 877-881.

[35] C.-H. Lee, M.-J. Hsieh, S.-H. Chang, Y.-H. Lin, S.-J. Liu, T.-Y. Lin, K.-C. Hung, J.-H.S. Pang, J.-H. Juang, Enhancement of Diabetic Wound Repair Using Biodegradable Nanofibrous Metformin-Eluting Membranes: in Vitro and in Vivo, ACS Appl. Mater. Interfaces 6 (2014) 3979-3986.

[36] Q. He, X. Zhang, B. Han, J. Xu, K. Tang, Z. Fu, H. Yin, A synergistic therapeutic scheme for hyperglycemia and nephrotic disorders in diabetes, Theranostics 4 (2014) 556-564.

[37] H. Alenezi, M.E. Cam, M. Edirisinghe, Experimental and theoretical investigation of the fluid behavior during polymeric fiber formation with and without pressure, Appl. Phys. Rev. 6 (2019) 041401.

[38] S.R. Gomes, G. Rodrigues, G.G. Martins, M.A. Roberto, M. Mafra, C.M.R. Henriques, J.C. Silva, In vitro and in vivo evaluation of electrospun nanofibers of PCL, chitosan and gelatin: A comparative study, Mater. Sci. Eng. C 46 (2015) 348-358.

[39] N. Satheeshkumar, S. Shantikumar, R. Srinivas, Pioglitazone: A review of analytical methods, J. Pharm. Anal. 4 (2014) 295-302.

[40] Y.D. Dange, S. Honmane, S. Bhinge, V. Rajaram Salunkhe, D. Raghunath Jadge, Development and Validation of UV-Spectrophotometric Method for Estimation of Metformin in Bulk and Tablet Dosage Form, Indian J. Pharm. Educ. 51 (2017) 754-760.

[41] N. Haq, F.K. Alanazi, I.A. Alsarra, F. Shakeel, Rapid Analysis of Glibenclamide Using an Environmentally Benign Stability-Indicating RP-HPLC Method, IJPR 13 (2014) 863-872.

[42] M Eltayeb, E.Stride, M.Edirisinghe, A.Harker, Electrosprayed Nanoparticle Delivery System for Controlled Release, Mater.Sci.Eng. C 66 (2016) 138-146.

[43] I. Toygar, A. Tureyen, D. Demir, S. Cetinkalp, Effect of allicin on wound healing: an experimental diabetes model, J. Wound Care 29 (2020) 388-392.

[44] O.M. El-Borady, M.S. Othman, H.H. Atallah, A.E. Abdel Moneim, Hypoglycemic potential of selenium nanoparticles capped with polyvinyl-pyrrolidone in streptozotocin-induced experimental diabetes in rats, in: Heliyon, 2020, pp. e04045.

[45] H.S. Mutlu, A. Erdoğan, L. Tapul, Autologously transplanted dermal fibroblasts improved diabetic wound in rat model, Acta Histochem. 122 (2020) 151552.

[46] S.L. Levengood, A.E. Erickson, F.-C. Chang, M. Zhang, Chitosan-Poly(caprolactone) Nanofibers for Skin Repair, J J. Mater. Chem. B 5 (2017) 1822-1833.

[47] M.E. Cam, S. Cesur, T. Taskin, G. Erdemir, D.S. Kuruca, Y.M. Sahin, L. Kabasakal, O. Gunduz, Fabrication, characterization and fibroblast proliferative activity of electrospun Achillea lycaonica-loaded nanofibrous mats, Eur. Polym. J. 120 (2019) 109239.

[48] M. Emin Cam, A. Nur Hazar-Yavuz, S. Cesur, O. Ozkan, H. Alenezi, H. Turkoglu Sasmazel, M. Sayip Eroglu, F. Brako, J. Ahmed, L. Kabasakal, G. Ren, O. Gunduz, M. Edirisinghe, A novel

treatment strategy for preterm birth: Intra-vaginal progesterone-loaded fibrous patches, Int. J. Pharm. (2020) 119782.

[49] S. Jian, J. Zhu, S. Jiang, S. Chen, H. Fang, Y. Song, G. Duan, Y. Zhang, H. Hou, Nanofibers with diameter below one nanometer from electrospinning, RSC Advances 8 (2018) 4794-4802.

[50] J. Xu, N. Cai, W. Xu, Y. Xue, Z. Wang, Q. Dai, F. Yu, Mechanical enhancement of nanofibrous scaffolds through polyelectrolyte complexation, Nanotechnology 24 (2013) 025701.

[51] S. Samimi Gharaie, S. Habibi, H. Nazockdast, Fabrication and characterization of chitosan/gelatin/thermoplastic polyurethane blend nanofibers, J. Text. Fibrous Mater. 1 (2018) 2515221118769324.

[52] G.M. Kim, K.H. Le, S.M. Giannitelli, Y.J. Lee, A. Rainer, M. Trombetta, Electrospinning of PCL/PVP blends for tissue engineering scaffolds, J. Mater. Sci. Mater. Med. 24 (2013) 1425-1442.

[53] V. Pandit, R. Pai, K. Devi, S. Suresh, In vitro-in vivo evaluation of fast-dissolving tablets containing solid dispersion of pioglitazone hydrochloride, J. Adv. Pharm. Technol. Res. 3 (2012) 160-170.

[54] Y.A. Chowdary, R. Raparla, M. Madhuri, Formulation and Evaluation of Multilayered Tablets of Pioglitazone Hydrochloride and Metformin Hydrochloride, J. Pharm. (2014) 1-14.

[55] M. Nurani, V. Akbari, A. Taheri, Preparation and characterization of metformin surface modified cellulose nanofiber gel and evaluation of its anti-metastatic potentials, Carbohydr. Polym. 165 (2017) 322-333.

[56] P. Ramalingam, Y. Reddy, K. Kumar, B. Chandu, K. Rajendran, Evaluation of metformin hydrochloride in Wistar rats by FTIR-ATR spectroscopy: A convenient tool in the clinical study of diabetes, J. Nat. Sci. Biol. Med. 5 (2014) 288-292.

[57] N.L. Delgadillo-Armendariz, N.A. Rangel-Vazquez, E.A. Marquez-Brazon, B. Rojas-De Gascue, Interactions of chitosan/genipin hydrogels during drug delivery: a QSPR approach, Química Nova 37 (2014) 1503-1509.

[58] Z. Wojnarowska, K. Grzybowska, K. Adrjanowicz, K. Kaminski, M. Paluch, L. Hawelek, R. Wrzalik, M. Dulski, W. Sawicki, J. Mazgalski, A. Tukalska, T. Bieg, Study of the Amorphous Glibenclamide Drug: Analysis of the Molecular Dynamics of Quenched and Cryomilled Material, Mol. Pharm. 7 (2010) 1692-1707.

[59] S. Gautam, C.-F. Chou, A.K. Dinda, P.D. Potdar, N.C. Mishra, Fabrication and characterization of PCL/gelatin/chitosan ternary nanofibrous composite scaffold for tissue engineering applications, J. Mater. Sci. 49 (2014) 1076-1089.

[60] X.-f. Qian, J. Yin, S. Feng, S.-h. Liu, Z.-k. Zhu, Preparation and characterization of polyvinylpyrrolidone films containing silver sulfide nanoparticles, J. Mater. Chem. 11 (2001) 2504-2506.

[61] M. Razavi, H. Karimian, C.H. Yeong, M. Fadaeinasab, S.L. Khaing, L.Y. Chung, D.E.B. Mohamad Haron, M.I. Noordin, Gastroretentive behavior of orally administered radiolabeled tamarind seed formulations in rabbits validated by gamma scintigraphy, Drug Des. Dev. Ther. 11 (2016) 1-15.

[62] A. Hemanth, Y. Anand Kumar, Preparation and Evaluation of Pioglitazone HCl Solid Dispersions, JChrDD 7 (2016) 73-82.

[63] D. Lucio, J.M. Irache, M. Font, M.C. Martinez-Oharriz, Supramolecular structure of glibenclamide and beta-cyclodextrins complexes, Int. J. Pharm. 530 (2017) 377-386.

[64] J. Zhan, Y. Morsi, H. Ei-Hamshary, S.S. Al-Deyab, X. Mo, In vitro evaluation of electrospun gelatin–glutaraldehyde nanofibers, Front. Mater. Sci. 10 (2016) 90-100.

[65] C.H. Lee, M.J. Hsieh, S.H. Chang, Y.H. Lin, S.J. Liu, T.Y. Lin, K.C. Hung, J.H. Pang, J.H. Juang, Enhancement of diabetic wound repair using biodegradable nanofibrous metformin-eluting membranes: in vitro and in vivo, ACS Appl. Mater. Interfaces 6 (2014) 3979-3986.

[66] W. Tighzert, A. Habi, A. Ajji, T. Sadoun, F.B.-O. Daoud, Fabrication and characterization of nanofibers based on poly(lactic acid)/chitosan blends by electrospinning and their functionalization with phospholipase A1, Fibers Polym. 18 (2017) 514-524.

[67] P.L. Ritger, N.A. Peppas, A simple equation for description of solute release, J. Control. Release 5 (1987) 23– 36.

[68] H.N. Hirapara, V.M. Ghori, A.P. Anovadiya, C.R. Tripathi, Evaluation of wound healing activity of cow urine ark in diabetic Wistar albino rats, J. Intercult. Ethnopharmacol. 5 (2016) 434-438.

[69] J.G. Merrell, S.W. McLaughlin, L. Tie, C.T. Laurencin, A.F. Chen, L.S. Nair, Curcumin-loaded poly(epsilon-caprolactone) nanofibres: diabetic wound dressing with anti-oxidant and anti-inflammatory properties, Clin. Exp. Pharmacol. Physiol. 36 (2009) 1149-1156.

[70] Y. Liu, S. Zhou, Y. Gao, Y. Zhai, Electrospun nanofibers as a wound dressing for treating diabetic foot ulcer, Asian J. Pharm. Sci. 14 (2018).

[71] L.J. Gould, Topical Collagen-Based Biomaterials for Chronic Wounds: Rationale and Clinical Application, Adv. Wound Care (New Rochelle) 5 (2016) 19-31.

[72] M.G. Tucci, G. Ricotti, M. Mattioli-Belmonte, F. Gabbanelli, G. Lucarini, F. Orlando, C. Viticchi, A. Bigi, S. Panzavolta, N. Roveri, G. Morganti, R.A.A. Muzzarelli, Chitosan and Gelatin as Engineered Dressing for Wound Repair, J J. Bioact. Compat. Polym. 16 (2001) 145-157.

[73] F. Xu, C. Zhang, D.T. Graves, Abnormal cell responses and role of TNF-α in impaired diabetic wound healing, BioMed Res. Int. 2013 (2013) 754802-754802.

[74] A.A.W. Sallam, A. El-Sharawy, Role of interleukin-6 (IL-6) and indicators of inflammation in the pathogenesis of diabetic foot ulcers, AJBAS 6 (2012) 430-435.

[75] R.E. Mirza, M.M. Fang, W.J. Ennis, T.J. Koh, Blocking interleukin-1β induces a healing-associated wound macrophage phenotype and improves healing in type 2 diabetes, Diabetes 62 (2013) 2579-2587.

[76] S.A. Eming, S. Werner, P. Bugnon, C. Wickenhauser, L. Siewe, O. Utermöhlen, J.M. Davidson, T. Krieg, A. Roers, Accelerated wound closure in mice deficient for interleukin-10, Am. J. Pathol. 170 (2007) 188-202.

[77] D.M. Nathan, J.B. Buse, M.B. Davidson, E. Ferrannini, R.R. Holman, R. Sherwin, B. Zinman, Medical management of hyperglycemia in type 2 diabetes: a consensus algorithm for the initiation and adjustment of therapy: a consensus statement of the American Diabetes Association and the European Association for the Study of Diabetes, Diabetes Care 32 (2009) 193-203.

[78] J.T. Lin, H.M. Chen, C.H. Chiu, Y.J. Liang, AMP-activated protein kinase activators in diabetic ulcers: from animal studies to Phase II drugs under investigation, Expert. Opin. Investig. Drugs 23 (2014) 1253-1265.

[79] M.T. Goova, J. Li, T. Kislinger, W. Qu, Y. Lu, L.G. Bucciarelli, S. Nowygrod, B.M. Wolf, X. Caliste, S.F. Yan, D.M. Stern, A.M. Schmidt, Blockade of receptor for advanced glycation end-products restores effective wound healing in diabetic mice, Am. J. Pathol. 159 (2001) 513-525.

[80] D.S. Straus, C.K. Glass, Anti-inflammatory actions of PPAR ligands: new insights on cellular and molecular mechanisms, Trends Immunol. 28 (2007) 551-558.

[81] S. Elshazly, E. Soliman, PPAR gamma agonist, pioglitazone, rescues liver damage induced by renal ischemia/reperfusion injury, Toxicol. Appl. Pharmacol. 362 (2019) 86-94.

[82] R.E. Mirza, M.M. Fang, M.L. Novak, N. Urao, A. Sui, W.J. Ennis, T.J. Koh, Macrophage PPARgamma and impaired wound healing in type 2 diabetes, J. Pathol. 236 (2015) 433-444.

[83] Y.W. Lin, P.S. Liu, K.A. Pook, L.N. Wei, Glyburide and retinoic acid synergize to promote wound healing by anti-inflammation and RIP140 degradation, Sci. Rep. 8 (2018) 834.

[84] P.C. Ho, L.N. Wei, Biological activities of receptor-interacting protein 140 in adipocytes and metabolic diseases, Curr. Diabetes Rev. 8 (2012) 452-457.

[85] P.S. Liu, Y.W. Lin, F.H. Burton, L.N. Wei, Injecting engineered anti-inflammatory macrophages therapeutically induces white adipose tissue browning and improves diet-induced insulin resistance, Adipocyte 4 (2015) 123-128.

[86] Y.W. Lin, B. Lee, P.S. Liu, L.N. Wei, Receptor-Interacting Protein 140 Orchestrates the Dynamics of Macrophage M1/M2 Polarization, J. Innate Immun. 8 (2016) 97-107.

Declaration of interests

X The authors declare that they have no known competing financial interests or personal relationships that could have appeared to influence the work reported in this paper.

☐The authors declare the following financial interests/personal relationships which may be considered as potential competing interests:

Author Statement

Muhammet Emin Cam: Conceptualization, Methodology, Validation, Writing - Original Draft. **Busra Ertas:** Methodology, Resources, Investigation. **Hussain Alenezi:** Writing - Original Draft, Validation, Formal analysis. **Ayse Nur Hazar-Yavuz:** Investigation, Writing - Original Draft. **Sumeyye Cesur:** Methodology, Resources, Investigation. **Gul Sinemcan Ozcan:** Investigation, Methodology, Writing - Original Draft. **Ceyda Ekentok:** Investigation, Methodology. **Ece Guler:** Investigation, Writing - Original Draft. **Christina Katsakouli:** Investigation, Writing - Original Draft. **Zehra Demirbas:** Investigation, Methodology. **Dilek Akakin:** Supervision, Writing - Original Draft. **Mehmet Sayip Eroglu:** Resources, Investigation, Writing - Original Draft. **Levent Kabasakal:** Visualization, Formal analysis. **Oguzhan Gunduz:** Resources. **Mohan Edirisinghe:** Visualization, Supervision, Project administration, Funding acquisition, Writing-Reviewing and Editing.

Click here to access/download
Supplementary Material
Supporting Information_MSEC_R1.pdf